Cinar, G., Cai, Y., Bendarkar, M. V., Burrell, A. I., Denney, R. K., & Mavris, D. N. (2023). System analysis and design space exploration of regional aircraft with electrified powertrains. Journal of Aircraft, 60(2), 382-409.

System Analysis and Design Space Exploration of Regional Aircraft with Electrified Powertrains

Gokcin Cinar*, Yu Cai†, Mayank V. Bendarkar‡, Andrew I. Burrell†, Russell K. Denney§ and Dimitri N. Mavris¶
Aerospace Systems Design Laboratory, School of Aerospace Engineering,
Georgia Institute of Technology, Atlanta, GA 30332

This paper explores the design spaces of a thin-haul and a regional aircraft with parallel hybrid-electric propulsion architectures for a 2030 entry into service date. Notional technology reference aircraft models were developed for a 19- and a 50-passenger aircraft based on publicly available data on Beechcraft 1900D and ATR 42-600, respectively. A set of airframe and propulsion system technologies projected to reach maturity by 2030 were infused into the aircraft models. Parametric, physics-based models were created for the charge depleting hybrid architecture. Different modes of operation were identified and parametrized with a range of design variables to investigate the feasibility and trade space for peak power shaving, climb power boosting, electric taxi, battery usage schedules, and in-flight battery recharge strategies. Thousands of electrified aircraft concepts with varying electrification, operation, and technology scenarios were sized under the same system-level requirements as their conventional counterpart. The resulting multidisciplinary design space exploration environment was used to identify the optimum vision system designs and modes of operation for the minimum block fuel burn objective. It has been found that both vehicle classes with the charge depleting parallel hybrid electric architecture provided fuel burn benefits over their 2030 advanced technology counterparts under certain operational modes.

I. Introduction

Electrified aircraft propulsion (EAP) is a disruptive technology that has the potential to significantly reduce, and even fully eliminate fuel consumption and aircraft emissions while allowing for more affordable and quieter flights [1]. However, there are also significant challenges including technological, regulative, and infrastructural barriers associated with this technology [2]. Even the most optimistic future battery technologies are unlikely to make complete electrification of commercial transport aircraft feasible in the near future [3]. Therefore, more attention is provided to

*Now: Assistant Professor of Aerospace Engineering, University of Michigan. *Previously:* Research Engineer II, Georgia Tech. AIAA Member.
†Senior Graduate Researcher, School of Aerospace Engineering, Georgia Tech, AIAA Student Member.
‡Research Engineer II, School of Aerospace Engineering, Georgia Tech, AIAA Member.
§Research Engineer II, School of Aerospace Engineering, Georgia Tech, AIAA Senior Member.
¶S.P. Langley Distinguished Regents Professor and Director of ASDL, School of Aerospace Engineering, Georgia Tech, AIAA Fellow.
Presented as AIAA Paper 2022-1994 at the AIAA SciTech 2022 Forum, San Diego, CA & Virtual, January 3–7, 2022.

the hybrid-electric aircraft concepts in literature. These typically use some form of a parallel and/or series powertrain arrangement with gas turbine engines as well as batteries to meet propulsive power and energy requirements. The term hybrid-electric is usually applied to aircraft with partial electrification of primary propulsive power, while complete electrification of the same is called an electric aircraft. Combined with novel architectures, these technologies can result in innovative concepts like the distributed electric aircraft that promise to reduce energy consumption and carbon emissions [4, 5]. However, these require additional efforts to characterize their off-nominal performance and safety [6, 7].

To aid the design of hybrid-electric aircraft, methods have been developed to estimate their range for a constant power-split ratio [8]. In a feasibility study, a hybrid-electric commercial transport aircraft was estimated to produce about half the lifecycle CO_2 of a conventional design [9].Pornet et al. estimated a fuel-burn reduction of up to 16% for a 900 nm reduced-range mission on a retrofit aircraft when using a 82:18 fuel-electrical energy mix [10]. Voskuijl et al. published a study on the design and analysis of a parallel hybrid electric regional turboprop aircraft [11]. They investigated two power management strategies for the hybrid electric powertrain, namely the constant power split and constant operating mode of gas turbine. The resulting design provided reduction in aircraft emissions when Lithium-air batteries with 1000 Wh/kg pack-level specific energy are used. However, the International Energy Agency's ETP Clean Energy Technology Guide estimates the current technology readiness level (TRL) of Lithium-air batteries as 1-2 [12], which means that they are not expected to be matured enough for aircraft applications by the 2030-2035 timeframe. Marien et al. [13, 14] presented a methodology and the results for electrified aircraft design exploration study, including 18-, 48- and 70-passenger turboprop aircraft. The results showed fuel burn savings for the electrified turboprop class aircraft with a pack level battery specific energy assumption of 500 Wh/kg. Jansen et al. proposed specific power and efficiency as the key performance parameters for turboelectric and hybrid electric aircraft to estimate the system level impact at early stage design [15, 16]. References [17–25], among many others, provided methods for early stage aircraft sizing and mission analysis. Parallel hybrid systems have been shown to provide some benefit in general aviation [23], regional turboprop [26], and narrow-body [27] class aircraft at even moderate battery energy densities.

In order to make a substantial effect on commercial aviation emissions, electrification must penetrate the single-aisle and wide-body markets due to the market share of these classes [28]. Additionally, EAP aircraft must have comparable ranges to aircraft they are replacing because the total aircraft emissions are dominated by longer range flights that an aircraft flies even though there are less of those flights. However, intermediate steps are needed to find solutions to the technological, regulative, and infrastructural challenges. The commuter and regional markets comprised of airliners that carry from 9 to 100 passengers are ideal candidates for transitioning to commercial aviation electrification. According to the Waypoint 2050 report published by Air Transport Action Group, the commuter and regional markets together are responsible of less than 4% of aviation-related CO_2 emissions [29]. However, the same report also states that the short haul market, comprising of 45-120 minute flights, is responsible for about 24% of the industry's CO_2 emissions. This means that a highly efficient hybrid regional airliner could be utilized in a larger market, and make a significant impact

on reducing the carbon emissions. Furthermore, if future electrified regional airliners have lower operating costs than the single aisle airliners, they could disrupt the hub and spoke system dominated by the single aisle vehicles.

The objective of this paper is to explore the design space for the thin-haul and regional vision systems with parallel hybrid electric propulsion system architectures for the NASA Electrified Powertrain Flight Demonstration (EPFD) program. Furthermore, it aims to identify the capabilities and trade-offs of different modes of operation to maximize the fuel-burn benefits of such systems. Compared to the studies found in literature, the power management strategy is varied within and across the flight segments to optimize the use of the parallel hybrid electric powertrain. The scope includes the development of parametric aircraft models for three stages of technology progression for each identified market segment: a technology reference baseline aircraft, a 2030 entry-into-service (EIS) advanced aircraft infused with the projected turbomachinery and airframe improvements, and the 2030 EIS EAP vision systems. This paper also aims to answer important questions about electrification, such as *when*, *how much*, and *how long* should the electrified systems be utilized in the design and operation of these systems. It brings a unique approach to parametrically modeling the modes of operation of the parallel hybrid electric propulsion system architecture. In contrast to the aforementioned work found in literature, this work seeks optimum design and operation solutions and does not assume constant hybridization factors.

This paper is part of a series of publications under the NASA EPFD project. It provides a framework for preliminary sizing of electrified turboprop aircraft. Related studies under the EPFD project provide a closer look at the conventional aircraft modeling with advanced technology [30, 31], modeling and simulation of parallel hybrid electric aircraft [32, 33], and turbine electrified energy management [34]. Other publications include future technology projections for electric machines [35], power electronics [36], batteries [37], and cables [38] for 2030 and beyond.

The following sections of this paper follow the four phases of this work: Section II briefly describes the integrated modeling and simulation environment used for this work. In Section III, a 19- and a 50-passenger technology reference aircraft are chosen to represent the state of the art of the thin-haul and regional market segments, respectively. The models were calibrated and validated against the publicly available data. In Section IV, airframe and propulsion system technologies are identified and selected based on their projected maturity levels for an EIS 2030 per vehicle class. A 19- and a 50-passenger 2030 advanced technology aircraft model are developed by infusing the selected technologies. These models form the basis of comparison against the EAP systems. Section V reports the parametric propulsion system models for the charge depleting parallel hybrid electric architecture based on the key performance parameters (KPPs). The EAP vision system concepts are then sized for the same point and mission performance requirements. The case for the parallel hybrid electric architecture and its modes of operation are also discussed at length in this section. Section VI reports how the parametric nature of all the models created enables extensive trade studies at the powertrain, aircraft, and mission levels. A design of experiments is conducted for each EAP vision system. Artificial Neural Network (ANN) models are created for the subsystem, system, and mission level metrics of interest. The ANN models are used to

explore the design space and find the optimum design and operation strategy for the minimum fuel burn aircraft. Finally, the resulting EAP vision system design points are compared against the 2030 advanced technology vehicles.

II. Modeling and Simulation Environment

A. Integrated Sizing and Synthesis Environment

The baseline, advanced, and EAP vehicles were modeled and sized using the multi-disciplinary analysis and optimization environment called Electrified Propulsion Architecture Sizing and Synthesis (E-PASS), developed by Cinar [39, 40]. E-PASS is a Matlab-based aircraft sizing and synthesis tool that enables the design and performance evaluation of conventional and advanced aircraft concepts with any type of propulsion system architecture. It utilizes an energy-based generic mission analysis approach where alternative energy storage systems can easily be integrated and analyzed within an advanced concept. The building blocks of E-PASS are shown in Fig. 1. It takes in a notional aircraft configuration (to geometrically scale the concept to) and top level aircraft requirements.

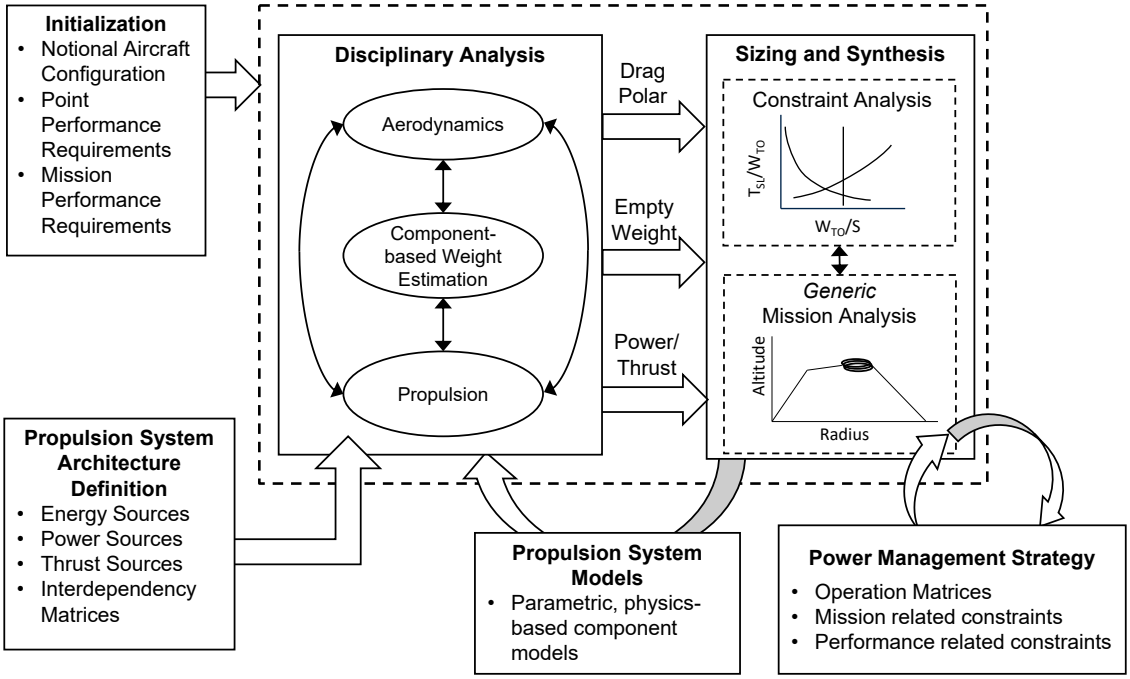

Fig. 1 Building blocks of the modeling and simulation environment: E-PASS [39]

E-PASS is powered by a unique methodology that categorizes propulsion subsystems in three general groups as originally proposed by Cinar [39, 40]:

- **Thrust Source:** any subsystem that generates thrust (e.g. propeller, fan, etc.)
- **Power Source:** any subsystem that generates primary (propulsive) power (e.g. internal combustion engine, electric motor, generator, etc.)
- **Energy Source:** any subsystem that stores energy to be used by the primary power sources (e.g. fossil fuel,

battery, hydrogen, etc.)

These three sources can be physically connected to each other to create *any* type of propulsion architecture using a graph theory-inspired approach. There exists an infinite number of possible connections, yielding a very large combinatorial architecture design space. This space can be conveniently described and explored by a set of matrices, namely the Interdependency Matrices, in the Propulsion System Architecture Definition block in Fig. 1. Thus, this methodology allows for the comparison between diverse propulsion architectures and their operations as part of the system level design and analysis.

Energy, power, and thrust sources in E-PASS are represented by parametric, physics-based models. This provides the capability to perform trade and multi-level optimization studies as well as technology projections and uncertainty quantification. Moreover, the Interdependency Matrices can be used within the propulsion system performance calculations so that the information propagation and power transmission between thrust, power, and energy source models are generalized and automated for any connection and architecture. This is a powerful approach as it completely removes the need to tailor the performance calculations to a specific architecture. The interested reader is referred to Ref. [40] for the mathematical framework upon which this novel approach is built. This approach is utilized within E-PASS, but the framework is tool-agnostic and can be used with any modeling environment.

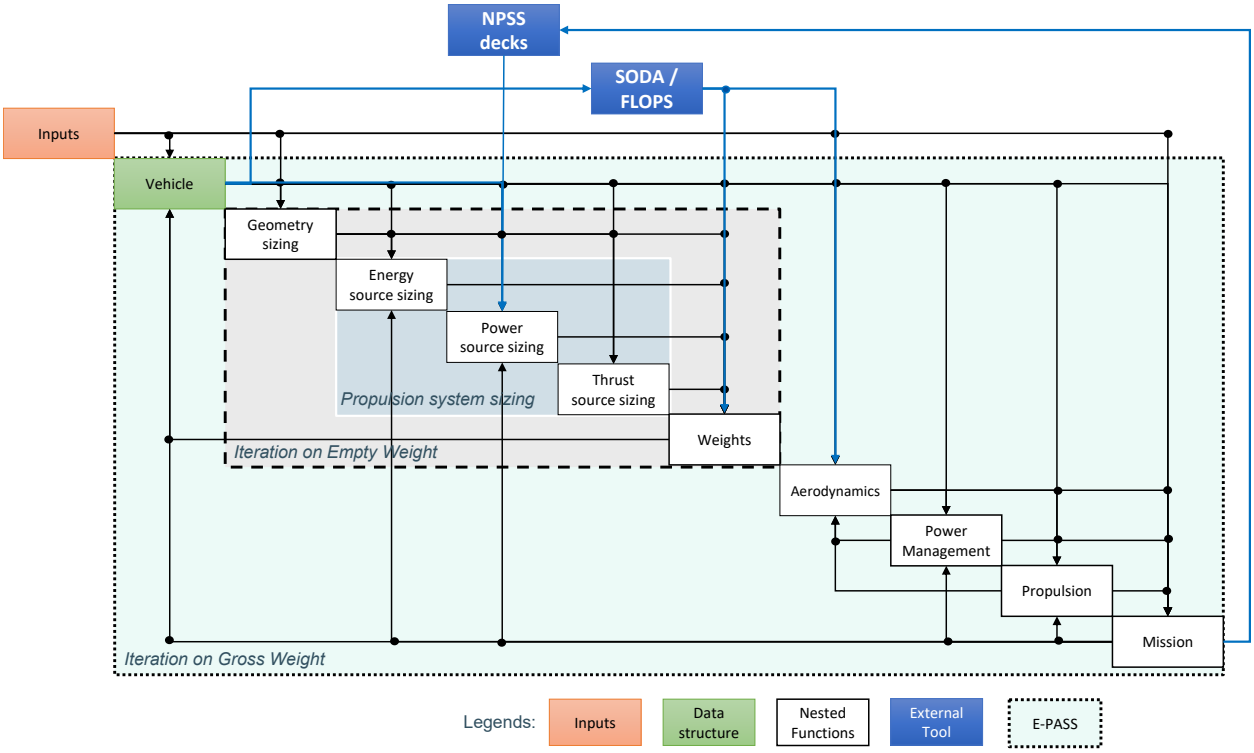

Fig. 2 High-level design structure matrix of the integrated multi-disciplinary analysis environment.

Once the propulsion architecture definition is created, its operation must be defined. For conventional architectures,

the operation strategy is straightforward as there is usually one type of thrust, power, and energy source employed. However, for unconventional architectures, there can be more than one power path that can be used in any given point of time in flight. There can also be different operation scenarios for different missions. In E-PASS, such decisions are made under the Power Management Strategy block. Similar to the architecture definition, the power management strategy is defined by Operation Matrices which consists of control points and power splits that define when and how available thrust, power, and energy sources are used. The power management strategy is explained in detail in Section V.

For this study, the Flight Optimization System (FLOPS) software [41] developed by NASA was integrated with E-PASS to provide the drag polar and the component-based empty weight estimations (except for the propulsion system weight). FLOPS uses a semi-empirical method [42] to estimate the weight of structural components and major subsystems, taking into account high-level geometry parameters, vehicle gross weight, and design payload-range. The integration was made possible by wrapping FLOPS using an in-house tool called SODA developed by Cai [43, 44];while SODA was initially created to use FLOPS to perform conceptual sizing and off-design mission analysis for aircraft with a conventional propulsion system, an improved interface was developed in this work to transfer data between FLOPS and E-PASS. The gas turbine engine core is modeled in NPSS. The NPSS engine model returns an engine deck which is then used by E-PASS during the mission analysis calculations. A high-level design structure matrix of this integrated sizing and synthesis environment is shown in Fig. 2.

B. NPSS Turboshaft Engine Models

To optimize the performance of a future hybrid electric aircraft, the turbine engine performance, size, and weight should be considered along with the other components of the vehicle. This capability is provided by a "scalable" turboshaft engine model, which predicts the expected performance and weight of new centerline engine designs over a continuous range of design power levels.

The scalable engine model was developed using the NASA Numerical Propulsion System Simulation (NPSS) [45]. To develop the model, first a "baseline" scalable engine model was built representing current engine data available from the open literature. The baseline model is not intended to match the performance of any specific engine(s), but to be representative of current engines with similar design power levels. All engines represented by the model are assumed to have the same architecture, i.e. a single spool gas generator with an axi-centrifugal compressor and a free power turbine, as shown in Fig. 3.

Next, the baseline model was adjusted to represent the expected performance and weight of future engines. Future performance trends were derived from several published sources, notably Snyder and Tong [46], Bettner [47], and Vogt and Sehra [48]. The engine cycle, defined by the design overall pressure ratio (OPR) and turbine inlet temperature (T4), is assumed to vary with engine design power. Performance improvements are assumed to be due to evolutionary improvements in component aerodynamics and turbine cooling as well as the incorporation of new technologies such

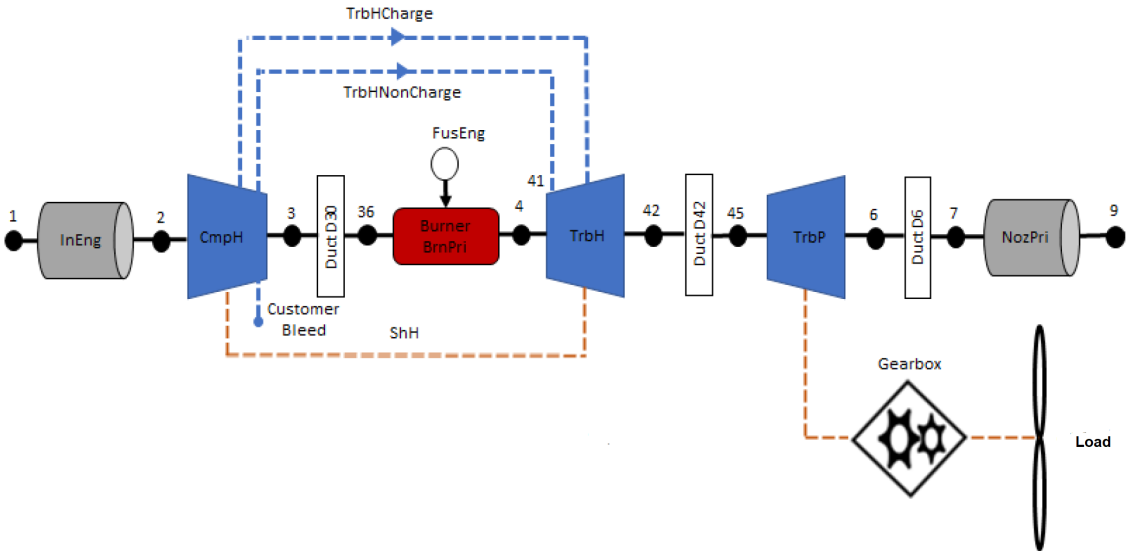

Fig. 3 Turboshaft engine diagram

as CMC materials and 3D manufacturing. Turbine cooling flows are estimated using the algorithm developed by Gauntner [49].

Figure 4 shows take-off brake specific fuel consumption (BSFC) vs. design shaft horsepower (SHP) predicted by the scalable engine model. The advanced engines have approximately 15% lower BSFC relative to current engines.

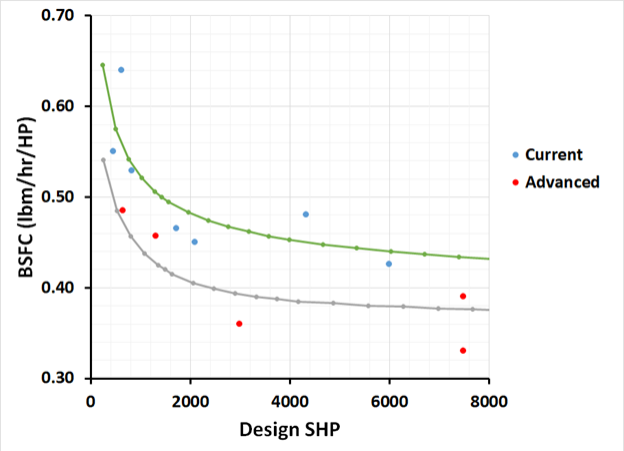

Fig. 4 Sea Level BSFC vs. Design SHP

The available data used to develop the model is quoted at sea level takeoff power, so this condition becomes the calibration point for the model. A multiple design point (MDP) method [50] is used to couple the top-of-climb power requirement to the sea level calibration point. The three design points are defined as follows:

- Sea level takeoff: calibration point; sets design power, OPR, and T4

- Hot day takeoff: engine power is flat-rated to a 95°F day; sets turbine cooling and T4 limit
- Top-of-climb: engine is sized to provide required power at TOC

The MDP design iteration begins with a guess for the sea level takeoff power. This value is used to select the design OPR and T4 from pre-defined correlation curves. The turbine cooling flows are sized at the hot day condition, which defines the maximum T4. The engine maintains maximum climb power until it becomes T4 limited at some altitude, at which point the power begins to decrease. The sea level power is iterated until the required top-of-climb power is achieved. The component design efficiencies are set at the TOC condition. After the engine design is established, off-design engine performance data is generated and provided to the vehicle system model. The entire process is repeated for a range of engine design power levels, as required during the vehicle level design iteration.

III. Technology Reference Aircraft Identification and Model Development

A. Technology Reference Aircraft Selection and Specification

Tables 1 and 2 present four candidates considered as the Technology Reference Aircraft (TRA) for the regional and the thin haul aircraft, sorted by the year of first flight. The TRA is selected based on the following criteria:

- **Technology level**: The selected aircraft should be equipped with technologies close to the current state-of-the-art; in this work, the technology level of the TRA is roughly estimated based on the year of first flight;
- **Data availability**: There should be sufficient data in the public domain to allow the authors to conduct appropriate calibration regarding its weight build-up and mission performance;
- **Market acceptance**: When multiple candidates satisfy the above two criteria, the one claiming a relatively high market share within its size class should be selected.

Table 1 Candidates for Thin Haul Turboprop Technology Reference Aircraft [51]

Candidate	Capacity	Configuration	Powerplant	First Flight	Number Built
Jetstream 31	19 pax	Low wing, cruciform tail	2x turboprop	1980	386
Dornier 228	19 pax	High wing, conventional tail	2x turboprop	1981	328+
Beechcraft 1900	19 pax	Low wing, T-tail	2x turboprop	1982	695
Cessna 408	19 pax	High wing, T-tail	2x turboprop	2020	1

Table 2 Candidates for Regional Turboprop Technology Reference Aircraft [51]

Candidate	Capacity	Configuration	Powerplant	First Flight	Number Built
DHC-7	50 pax	High wing, T-tail	4x turboprop	1975	113
ATR 42	48 pax	High wing, T-tail	2x turboprop	1984	457+
DHC-8-300	50 pax	High wing, T-tail	2x turboprop	1987	267
Saab 2000	50 pax	Low wing, conventional tail	2x turboprop	1992	63

1. Specifications of Thin Haul Turboprop Technology Reference Aircraft

Among the thin haul turboprops listed in Table 1, the Cessna 408 SkyCourier has the highest technology level; however, it is still undergoing flight testing with limited publicly available data for calibration. The remaining three candidates were developed around the same time frame. Therefore, based on the market share, the latest variant of Beechcraft 1900, the B1900D, is selected as the TRA.

The B1900D is the latest and most popular variant of the B1900 family. Entering commercial services in the 1990s, the B1900D is equipped with two PT6A-67D turboprop engines (certified in 1994) [52], and is able to carry 19 passengers over a distance of 382 nmi. The specifications of the B1900D used for model calibration are presented in Table 3. The mission profile is briefly described as follows, where an asterisk (*) denotes segments without distance credit:

1) **Taxi-out***: taxi for 10 min
2) **Takeoff***: take off and initial climb from sea level to 1000 ft for 1 min with active power sources operating at full power
3) **Climb**: climb to 20 000 ft at 160 KEAS
4) **Cruise**: level cruise at 275 KTAS
5) **Descent**: descend to sea level at 200 KEAS
6) **Altn Clb**: missed approach and climb to 15 000 ft at 160 KEAS
7) **Divert**: level cruise at 275 KTAS
8) **Altn Desc**: descend to 5000 ft at 200 KEAS
9) **Reserve***: level cruise at 200 KEAS for 45 min
10) **Altn Appr***: descend to 1500 ft while decelerating to 180 KEAS
11) **Landing***: landing at sea level for 1 min with active power sources operating at 40% of full power
12) **Taxi-in***: taxi for 5 min

The primary mission (segments 1-5 and 11-12) has a total distance of 382 nmi, and the cumulative fuel consumption is the block fuel. The reserve mission (segments 6-10) has a total distance of 100 nmi. The total fuel consumption of all segments is the required fuel of the design mission.

2. Specifications of Regional Turboprop Technology Reference Aircraft

Among the aircraft listed in Table 2, the ATR 42, DHC-8, and Saab 2000 were initially developed in the 1980s and were superior in terms of technology level compared to the DHC-7. However, the ATR 42 is the only type still in production, with its latest variant, the ATR 42-600, entering commercial services in the 2010s. Therefore, the ATR 42-600 is selected as the TRA.

The latest ATR 42-600 features essentially the same airframe design and seating capacity as the original ATR 42 in

Table 3 General Specifications of Selected Technology Reference Aircraft

Item	Thin Haul Airliner	Regional Airliner
Reference aircraft	B1900D	ATR 42-600
Design payload (kg)	1900 (19 pax)	4560 (48 pax)
Design range (nmi)	382	801
Wing loading (kg/m^2)	287	342
Power-to-weight ratio (kW/kg)	0.239	0.200
Maximum takeoff weight (kg)	7815	18 600
Operating empty weight (kg)	4847	11 700
Fuselage length (m)	17.6	22.7
Wing planform area (m^2)	27.2	54.5
Wing span (m)	16.5	24.6
Wing aspect ratio	10.0	11.1
Wing taper ratio	0.418	0.492
Wing quarter-chord sweep (deg)	0	2.3
Horizontal tail planform area (m^2)	6.32	11.4
Vertical tail planform area (m^2)	4.86	16.2
Powerplant	2x PT6A-67D	2x PW127M
Rated power, each (kW)	934	1864
Propeller diameter (m)	2.79	3.93
Propeller blades	4	6

the 1980s, with some improvements in the aerodynamic characteristics, avionics, and cabin design. It is equipped with two PW127M (certified in 2007) turboprop engines [53] which are de-rated to the same power as the PW127E, and is able to carry 48 passengers over a distance of 801 nmi [54]. The specifications of the ATR 42-600 used for model calibration are presented in Table 3. The mission profile is briefly described as follows, where an asterisk (*) denotes segments without distance credit:

1) **Taxi-out***: taxi for 10 min
2) **Takeoff***: take off and initial climb from sea level to 1500 ft for 1 min with active power sources operating at full power
3) **Climb**: climb to 25 000 ft at 160 KEAS
4) **Cruise**: level cruise at 300 KTAS
5) **Descent**: descend to 3000 ft at 200 KEAS
6) **Approach***: descend to 1500 ft while decelerating to 160 KEAS
7) **Altn Clb**: missed approach and climb to 10 000 ft at 160 KEAS
8) **Divert**: level cruise at 200 KEAS
9) **Reserve***: level cruise at 200 KEAS for 45 min

10) **Altn Desc**: descend to 3000 ft at 200 KEAS

11) **Altn Appr***: descend to 1500 ft while decelerating to 160 KEAS

12) **Landing***: landing at sea level for 1 min with active power sources operating at 40% of full power

13) **Taxi-in***: taxi for 5 min

The primary mission (segments 1-6 and 12-13) has a total distance of 801 nmi, and the cumulative fuel consumption is the block fuel. The reserve mission (segments 7-11) has a total distance of 87 nmi. The total fuel consumption of all segments is the required fuel of the design mission.

B. Technology Reference Aircraft Model Calibration, Results, and Validation

The TRA models are calibrated against the reference data in Table 3. The wing loading and power-to-weight ratio of the baseline aircraft were maintained to approximately meet the same point-performance requirements. The maximum takeoff weight (MTOW), geometry data, and engine deck are first specified in E-PASS, which calls FLOPS to estimate an operating empty weight (OEW) and a drag polar. A multiplicative scaling factor is then used to adjust the computed OEW until it matches the reference value. With the MTOW, calibrated OEW, and uncalibrated drag polar, E-PASS virtually flies the design mission to estimate the total fuel required. Another multiplicative scaling factor is then used to adjust the drag polar until the total fuel required matches the fuel available based on weight constraints. The scaling factors, vehicle sea level takeoff power-to-weight ratio, and wing loading are held constant in the subsequent vehicle resizing analyses.

After calibration, the TRA models are evaluated at a few off-design missions for testing. The off-design missions were modeled based on publicly available data published in Ref. [54, 55]. Tables 4 and 5 summarize the results of calibration and testing, based on which the calibrated models are considered to be good enough to represent the TRA.

Table 4 Calibration and validation of 19-pax TRA Model

Item	Reference [55]	TRA Model	Error
Maximum takeoff weight (kg)	7815	7815	–
Operating empty weight (kg)	4847	4847	–
Engine rated power (kW)	934	934	–
Wing planform area (m^2)	27.2	27.2	–
Range at max payload (nmi)	133	142	6.77 %
Ferry range (nmi)	1245	1234	−0.88 %

Table 5 Calibration and validation of 50-pax TRA Model

Item	Reference [54]	TRA Model	Error
Maximum takeoff weight (kg)	18 600	18 600	–
Operating empty weight (kg)	11 700	11 700	–
Engine rated power (kW)	1864	1864	–
Wing planform area (m^2)	54.5	54.5	–
Block fuel, 200 nmi mission (kg)	565	582	3.05 %
Block fuel, 300 nmi mission (kg)	783	780	−0.41 %

IV. Advanced Technology Aircraft Model Development

The electrified aircraft aims at an entry-into-services by the year of 2030, when some novel technologies for airframe and turboprop engines will also become mature. In order to isolate the impact of electrification, it is necessary to first establish an advanced technology aircraft model for each size class, which shall carry the applicable 2030 technologies while maintaining the conventional propulsion system architecture. This section gives a brief overview of the selected technologies and vehicle-level impacts on the reference aircraft.

A. Viable Technology Identification, Selection and Infusion

To create reference 2030 aircraft models, technologies are considered from the technology portfolio of the NASA Advanced Air Transport Technology project [56]. These are then filtered to ensure only those technologies that are expected to reach a TRL of 9 by 2030 are downselected, taking care to exclude any incompatibilities. Cost effectiveness and practicality for each seat class were also considered in the selection. A list of technologies infused into the 2030 baselines is given in Table 6.

Table 6 Technologies considered for 2030

Application Area	Technology	Benefit	TRL 9 Year	Implementation	
				50 Pax	19 Pax
Lifting Surfaces	Riblets [56, 57]	Aerodynamics	2028	x	
Wing	Variable-Camber Continuous Trailing-Edge Flap [56]	Weight, aerodynamics	2028	x	
Wing	Flexible Skins [56]	Aerodynamics	2028	x	
Aircraft	Advanced Sandwich Composites [56]	Weight	2020	x	
Aircraft	Composite Technologies (RTC) [56]	Weight	2020	x	x
Aircraft	Out-of-Autoclave Composite Fabrication [56]	Weight	2020	x	
Aircraft	Excrescence Reduction [56]	Aerodynamics	2020	x	x
Landing Gear	Landing Gear Integration [56]	Noise	2026	x	
Engine	Advanced Engine Cycle (ASDL Generated)	Fuel burn	2030	x	x
Engine	Advanced Engine Components	Fuel burn, weight	2030	x	x

B. 2030 Advanced Aircraft Model Results

To infuse the 2030 technologies onto the 50-pax baseline, the vehicle is resized while keeping constant power-to-weight ratio, wing loading, mission profile, and design payload-range. Each airframe technology is modeled as one or more multiplicative factors acting on intermediate results in FLOPS such as the structural component weights and drag components, while the engine technologies are modeled by directly adjusting the cycle parameters in NPSS. The impact of the selected technologies at the system level were modeled following the methodology described in the Technology Impact Matrix section of Ref. [58]. For the 19-pax, a similar procedure is followed except for an increase in the design payload, where the total weight per passenger is increased by 5 lb (2.3 kg) to comply with the latest FAA advisory circular.

The relatively large improvement in fuel burn of the advanced engine over the baseline engine may be explained by two factors. First, a different NPSS engine model, not the scalable engine model described previously, was used for the baseline engine performance. Differences between the baseline engine model and the scalable engine model run at current tech levels represent differences between the PW127-specfic engine model and the average current engine represented in the scalable engine model. The approximate relative differences in brake specific fuel consumption (BSFC) at design power between the baseline engine model, the scalable engine model run at current tech levels, and the scalable engine model run at advanced tech levels are illustrated in Fig. 6.

Second, the technology improvements assumed in the advanced tech engines not only represent evolutionary improvements in component efficiencies and turbine temperature limits, but the advanced engines are also designed to a higher compressor pressure ratio. The higher pressure ratio yields additional improvements in specific fuel consumption and also has a compounding effect on the vehicle performance, since it makes the engines smaller and lighter.

V. Electrified Aircraft Propulsion Model Development

The thin-haul and regional commuters present relatively more short-term opportunities for electrification compared to larger jets. This paper investigates the feasibility and benefits assessment of a charge depleting parallel hybrid electric architecture on the 19 and 50 passenger class EAP vision systems. This parallel architecture uses electric machines to supplement the thermal core power of the turbine engine. It has the ability to provide a substantial fraction of power in all-electric and hybrid modes. This architecture is notionally demonstrated in Fig. 7. This parallel architecture is very similar to those in Ref. [23, 26].

The 19- and 50-pax EAP vision systems employ a parallel hybrid electric powertrain on each wing. The battery pack which includes the cells, housing, cooling, battery management system, and module wiring is placed in the fuselage. The electric energy is distributed via cables from the battery to the bus, and then to the electric motors on each side of the wing. The electric motor and turboshaft engine on each side is connected to the propeller shaft via a power split unit.

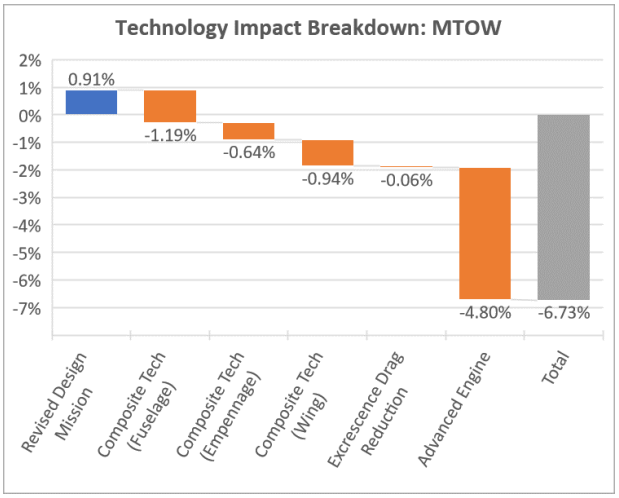

(a) 19-pax MTOW

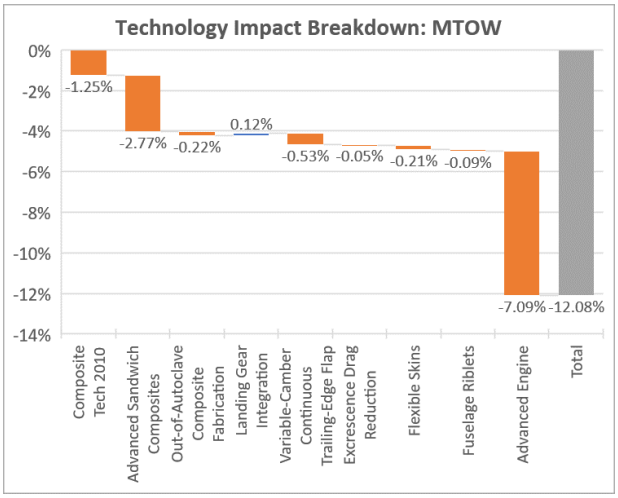

(b) 50-pax MTOW

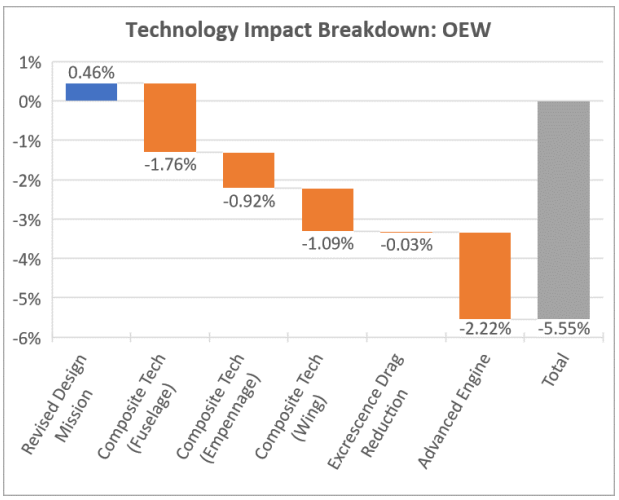

(c) 19-pax OEW

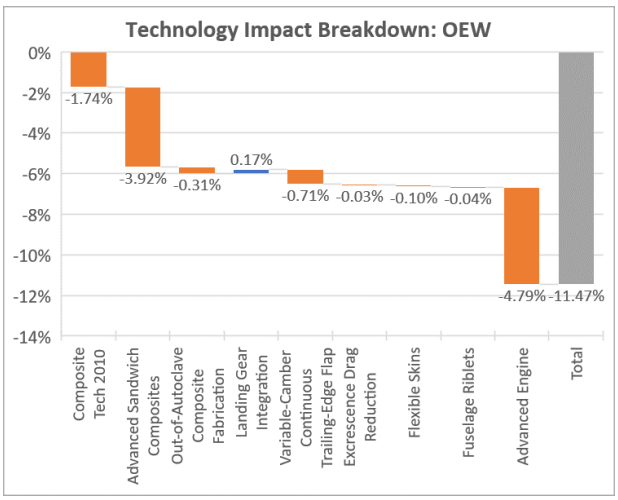

(d) 50-pax OEW

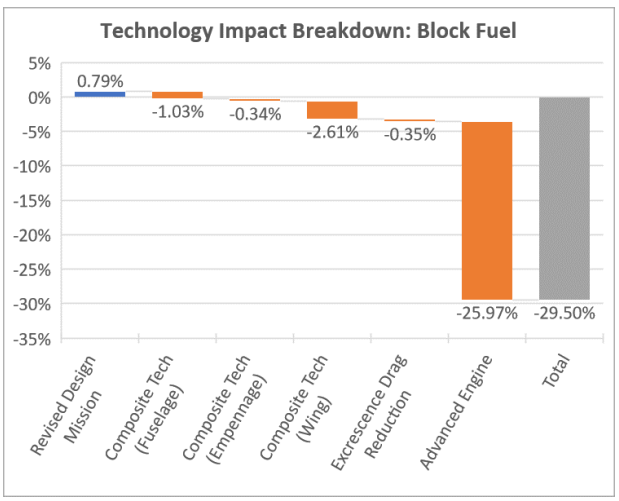

(e) 19-pax Block Fuel

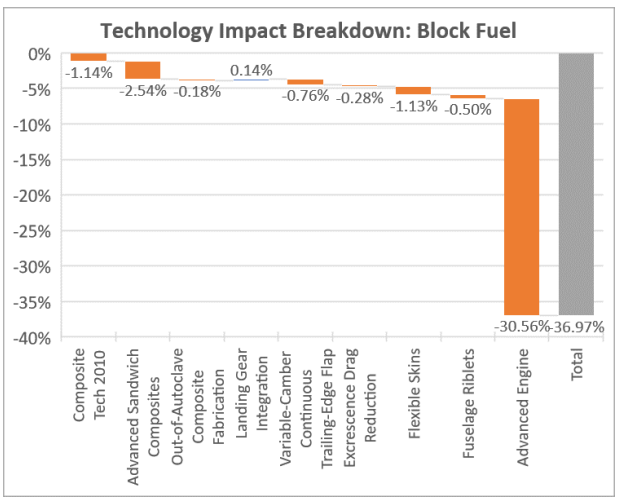

(f) 50-pax Block Fuel

Fig. 5 Impact of preliminary technology infusion on the two baselines

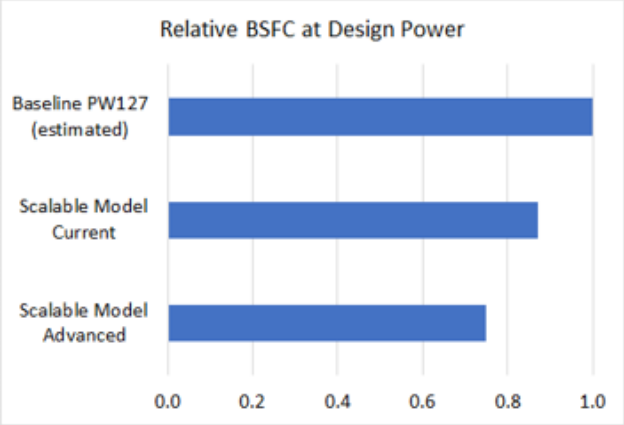

Fig. 6 Relative BSFC (lbm/hr/HP) at design power.

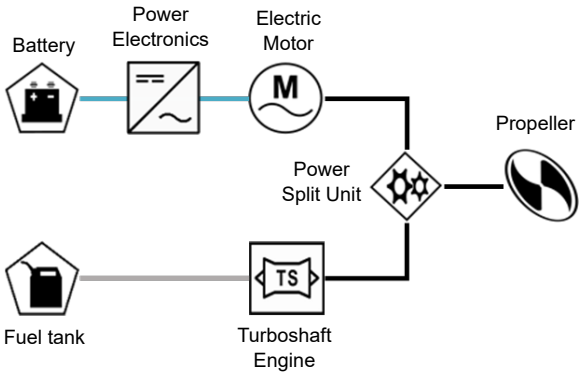

Fig. 7 Notional parallel hybrid electric architecture.

A. Modes of Operation for the Parallel Hybrid Electric Architecture

This parallel hybrid electric architecture enables the following modes of operation: peak power shaving, climb boosting, cruise hybridization, electric taxi (e-taxi), in-flight battery recharging. In this phase of research, the EAP vision systems utilize peak power shaving and power boosting during takeoff and climb segments. The taxi out segment is fully electrified. The battery is recharged during cruise and/or descent segments. These operating modes allow designers to maximize the impact of parallel electric architecture from Fig. 7 and are a unique contribution of this work. A detailed explanation to each considered approach and the reasons for the decisions and assumptions made are provided in the following paragraphs.

1. Engine peak power shaving

For the 19- and 50-pax TRA and advanced aircraft, the sizing point for the turboprop engine is obtained at takeoff conditions. In a parallel hybrid electric architecture, the electric motors can be used to provide partial power during takeoff. This means that under otherwise identical conditions, a smaller engine core with a lower peak power would

suffice to maintain the same aircraft takeoff performance. In other words, the peak power of the engine can be "shaved" by downsizing the engine.

The two main benefits of the power shaving strategy are the reduced weight of the engine, and the increased fuel burn efficiency during cruise, as discussed by Spierling and Lents [26]. The latter comes from the fact that a smaller engine in a parallel hybrid electric architecture can be operated at or near the peak power during takeoff, climb and cruise. The engine core is most efficient when it is operated at the peak power settings. Thus, a higher thermal efficiency is expected for a longer duration of the flight. Consequently, this could result in a reduction in mission fuel burn. Note that the engine peak power can be shaved up to the cruise power requirement unless the cruise segment is also hybridized.

2. Climb power boosting

The electric motor connected in parallel to the turboshaft engine can provide full or partial power during the climb segment to either provide additional propulsive power or to offset some of the engine power. Power offset requires de-rating the engine which is not always desirable from a climb performance and thermal efficiency perspective. On the other hand, power boosting might be advantageous in certain cases. Electric machines do not lapse with altitude as opposed to internal combustion engines. Thus, they bring a performance advantage that can be used to reduce time to climb. This can eventually bring additional fuel burn savings. However, depending on the motor size, full power throughout the climb might not always be necessary or beneficial because the power required decreases as the climb progresses. Furthermore, the amount and duration of electric power boost (also referred to as "e-boost") heavily impacts the battery capacity. The higher the capacity, the heavier the battery and the aircraft becomes, requiring more power to take off and climb at the desired performance levels. This tradeoff is carefully studied in this paper.

3. Electric taxi (e-taxi)

Thin haul and regional aircraft are mostly utilized in small airports which typically do not have heavy traffic. This results in relatively short taxi in and out times compared to larger transports. According to the Georgia Tech team's inquiries with ATR-42 pilots, the taxi time ranges between 5-10 minutes and the variation depends on the size or congestion of the airport. The ATR-42 brochure in Ref. [59] also quotes a 4 minute taxi allowance.

However, fuel burned during taxi is still significant and the resulting emissions contribute to local air pollution at airports. Using electric power to drive the aircraft to the runway can provide significant environmental benefits. To this end, two e-taxi approaches have been considered: the first approach is to implement an additional electric motor to electrically power the landing gear wheels for movement during ground operations. This approach was not chosen for this study due to the additional weight that would be brought to the system by the electric motor(s). The second option is to use one or both of the electric motors that already exists on the parallel hybrid architecture to drive one or both of the propellers and carry out the ground operation through thrust generated by the propellers. The electric motors are

also highly efficient at a wide range of torque and speed conditions, as opposed to the turboshaft engine which is much less efficient at low throttle settings.

4. Cruise hybridization

This architecture can be used in hybrid mode during the cruise segment to reduce the aircraft emissions at cruise altitudes. However, even small hybridization could require a very heavy battery due to the long cruise times and the low gravimetric specific energy of batteries projected for 2030. This means that the aircraft must take off, fly, and land at higher weights which could easily diminish the benefits. Thus, cruise hybridization was not considered in this study. However, cruise hybridization can be feasible for shorter and/or lighter missions. Although off-design flight performance and hybridization strategies are not in the scope of this paper, an example case for cruise hybridization is given here: a shorter range (and/or lighter payload) mission would require less energy to reach top of climb (which can be at a lower altitude than the design cruise altitude), leaving the state of charge of the battery above its minimum limit. Then, this available energy in the battery can be used to off-set the engine cruise power. As such, different hybridization strategies can be tailored for different points in the payload-range diagram of an aircraft.

5. In-flight battery recharge

The battery must have sufficient charge at the beginning of each mission. The design mission analysis made in this study assumes 100% State of Charge (SoC) at the beginning of the mission. It is possible for some shorter range off-design missions to carry out multiple missions before fully charging the battery, or the battery can be partially charged at the end of each mission. However the battery must be fully recharged before flying the longer range missions which requires full battery capacity.

There are two options for recharging the battery: on-ground recharging and in-flight recharging. In the first scenario, the battery must be charged at the gate in between operations. The time required to charge the battery depends on the battery capacity and charging C-rate. If the charging rate is low, then the time spent at the gate can be longer than acceptable for airlines. On the other hand, safe high-rate charging capability requires infrastructure changes. Although some airports might have the necessary infrastructure to support fast-charging at the gate, not all regional airports might be able to implement it by 2030.A short-term solution until the necessary infrastructures are built is to charge the battery during flight using the turbine engines. In the case of this parallel hybrid electric architecture, the electric motors are used in generator mode to convert the mechanical energy coming from the turbine shaft to electric energy to charge the battery. Clearly, the turboshaft engines must operate at higher power settings to charge the batteries. This can result in increased fuel burn which, in some cases, can diminish the benefits of electrification. In other cases, running the engine at a higher power setting could increase thermal efficiency. As discussed earlier, there are thermal limits on the maximum charging rates of the battery. As a trade study, this paper investigates battery charging during cruise and/or

descent segments. Other charging technologies such as windmilling are out of scope of this phase of the research.

The following sections describe a novel methodology for component modeling, mission profile modeling, and aircraft sizing and synthesis. This methodology is specifically developed to study the combinatorial design space of the selected operational modes parametrically.

B. Electric Powertrain Component Modeling

The electric powertrain consists of an electric machine, power converter, electric cables, DC bus, and battery. These components were modeled parametrically in E-PASS in terms of their power/energy capabilities, efficiency, and weights.

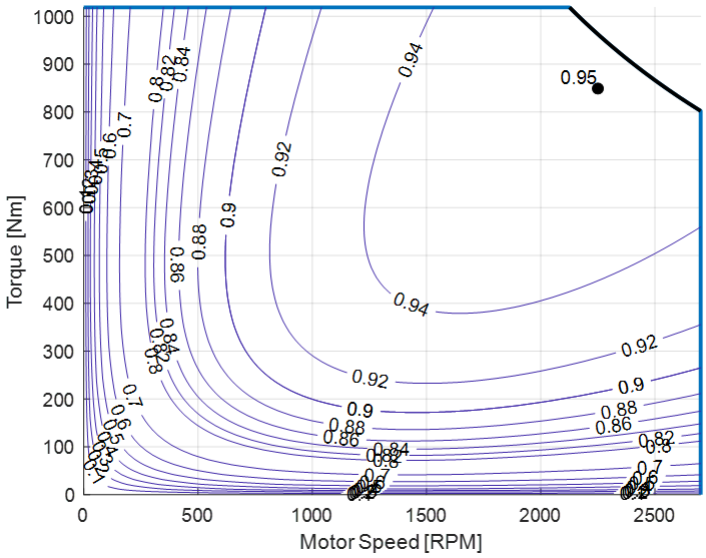

Fig. 8 Example electric motor model described by the efficiency curves and the motor torque and speed envelope.

The electric machine functions as a motor (when the battery is being discharged) and a generator (when the battery is being charged). A parametric, loss-based electric motor model had been developed based on Larminie and Lowry [60]. This model builds up efficiency maps based on Coulomb frictional, windage, iron, copper, and parasitic losses in an electric motor. An example efficiency map as a function of motor torque and speed is given in Fig. 8. It requires maximum power, maximum efficiency, design speed, design power, and max-to-design ratios of torque and speed as inputs. Some of these inputs were varied in the trade studies to reflect different technology levels, while others were determined based on mission and performance requirements and state of the art, aviation-grade electric motors. The model coefficients were also manipulated within the aircraft sizing process so that the highest motor efficiency falls into the torque-speed setting where the motor is utilized for the longest period of time. The electric machine speed-voltage and torque-current relationships were defined via the back-EMF constant, which is selected to ensure that the electric machine voltage is within the operating range of the power converter. The electric machine weight is calculated based on specific power and maximum power.

The power converter model functions as both an inverter and rectifier. The AC voltage and current are governed by the electric machine, while the DC voltage is dictated by the motor cable. The power converter weight is calculated based on specific power and maximum power.

The parametric battery model was developed based on the work published by Tremblay and Dessaint [61]. The model takes in cell unit information, and sizes the pack for high level requirements such as capacity and voltage. The baseline cells were modeled after Samsung INR18650-30Q cells, which are used on the X-57 Maxwell aircraft. The baseline battery cell parameters are given in Table 7. The baseline battery cell discharge and recharge curves at 3A created using this model are shown in Fig. 9. Additionally, correction factors were added to the baseline battery cell model to customize voltage and capacity. These correction factors can accommodate different battery cell sizes like Tesla's 2170 and 4680 cells. The maximum and minimum limits of the battery state of charge are 100% and 20%, respectively.

Table 7 Baseline battery cell parameters.

Battery Parameter	Value
Nominal Capacity (Ah)	3.0
Nominal Voltage (V)	3.6
Max Continuous Current (A)	15
Cell Specific Energy (Wh/kg)	225
Weight (g)	48

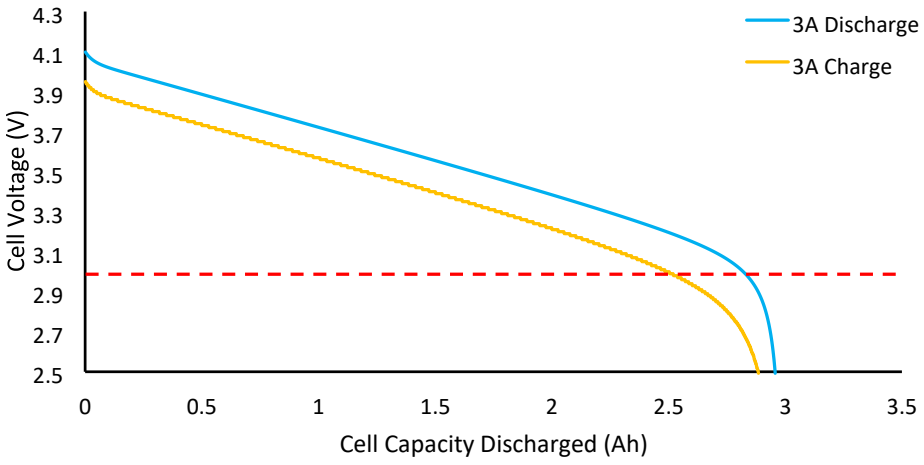

Fig. 9 Baseline cell discharge and recharge curves.

The battery pack is built from cells contained in series and parallel connected modules. The stack voltage is calculated from the product of the cell voltage and number of cells in series. The pack capacity is calculated from the product of cell capacity and number of cells in parallel. The number of parallel and series connected cells per module

were selected as trade study variables, due to their impact on the weight of the battery. The battery pack voltage is equal to the system voltage, which is also a trade study variable. The battery pack weight consists of the cell weight and packaging weight. The cell weight is calculated from the cell-level specific energy and design energy capacity. Packaging weight is calculated based on the number of modules, module cell configuration, and component weights. A technology factor is added to the packaging weight to allow the pack-level specific energy to be modified independently from the cell-level specific energy.

The electric cables are designed via a required efficiency, which is used to determine the resistance and required total conductor area. The weight is built up from cable components including the conductors, insulation, magnetic shielding, and cooling jacket, while also accounting for void space between components [62, 63]. The contribution of each component to the linear mass density of the cable as a function of battery stack voltage is given in Fig. 10 for a 150 kW and a 1.2 MW electric motor power. These cables connect the motor and the battery to the electric bus.

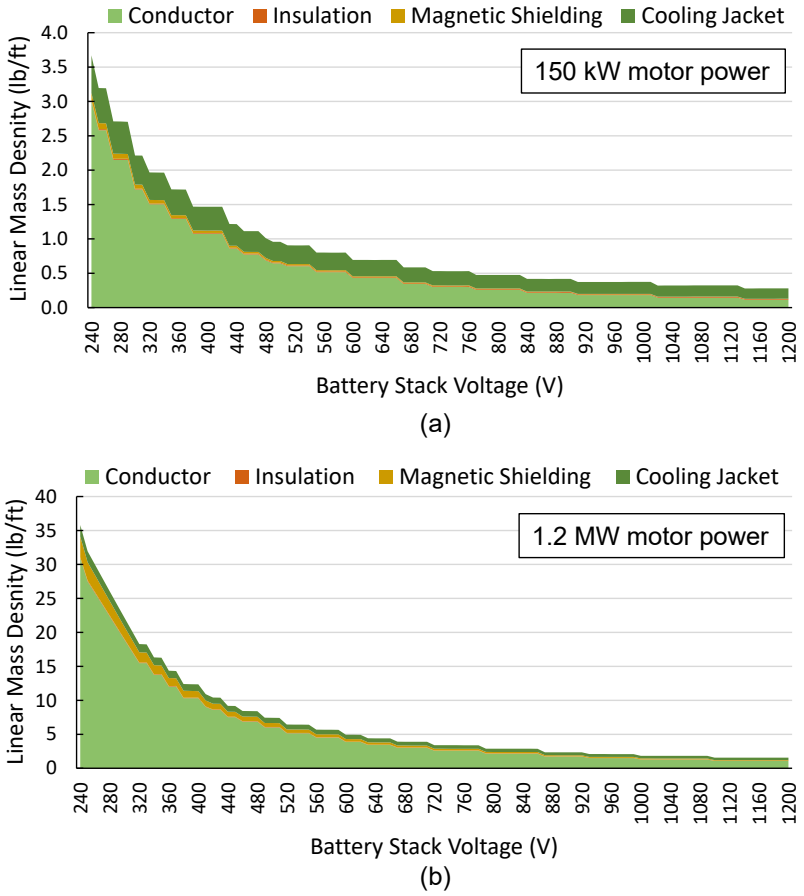

Fig. 10 Contribution of each component to the linear mass density of the cable as a function of battery stack voltage for (a) 150 kW power electric motor, and (b) 1.2 MW power electric motor.

The electric powertrain component assumptions made for these analyses are given in Table 8. The technology related assumptions represent the predictions for 2030-2035 EIS made for the scope of this work. Note that although the

cell-level battery specific energy was kept at 0.5 kWh/kg, the pack-level specific energy changes based on packaging, which in turn is affected by system voltage and number of series and parallel cell connections per module.

Table 8 2030 electrified powertrain technology assumptions.

Component	Parameter	Value
Battery	Cell specific energy	500 Wh/kg
	Cell density	2805 kg/m^3
	Packaging weight factor	0.45
	Cell voltage	4.088 V
	Max cell current	15 A
	Cell capacity	3 Ah
Cable	Efficiency	99.6%
	Length for 19-pax (battery – bus)	25 ft
	Length for 50-pax (battery – bus)	40 ft
	630 Amp ampacity conductor diameter	35.916 mm
Power converter	Efficiency	98.0%
	Specific power	16.4 kW/kg
Electric machine	Max efficiency	96.0%
	Specific power	13.0 kW/kg
Bus	Efficiency	100%

C. Electrified Propulsion Architecture Sizing and Synthesis

The energy, power, and thrust source sizing were carried out in E-PASS in-line with the aircraft sizing process. This section provides details as to how these components were sized for the EAP vision system. The same technical approach was used for the TRA and advanced vehicles, except that they did not have the electric powertrain components in the process. For these platforms, thrust source refers to the propellers, power sources refer to the engine and the motor, and the energy sources refer to the fuel and the battery. E-PASS first starts with an initial guess for the propeller diameter and speed, engine and motor power, as well as fuel and battery capacity. The energy-based mission analysis is carried out with these initial values.

1. Energy source sizing

The energy source sizing includes the calculation of the required fuel mass and the battery capacity. This information comes from the energy-based mission analysis. The required fuel mass is calculated from the fuel flow calculated at each time step of the mission as obtained from the engine deck. The required battery capacity is calculated by the electrical power demanded by the electric machine at each time step. The power flow during the mission is calculated based on the power management strategy which must be determined a-priori. Figure 11 demonstrates the electric power flow paths on the electric powertrain during battery discharge and charge modes. The battery is sized based on the amount

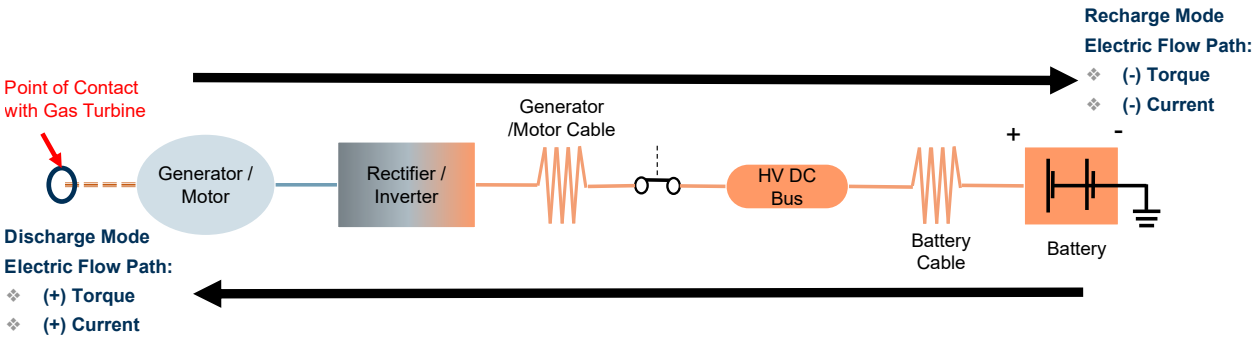

Fig. 11 Electric power flow paths on the electric powertrain during battery discharge and charge modes. The amount and direction of power being propagated depends on the required shaft power and the power management strategy.

of net energy required for the discharge schedule. Figure 12 shows a high-level process chart for the battery sizing process. The user-defined power management strategy includes a battery usage schedule which contains information about *when*, for *how long*, and *how much* the battery will be discharged. The timing and the duration of the discharge are defined in terms of the mission segment and the range of altitudes where the battery will be discharged. Specifying the battery operation in terms of an altitude range is especially useful for partial climb discharging. The amount of power to be discharged from the battery comes from the electric motor power code (i.e. power setting) which is defined as the percent maximum motor power. Then, this power requirement is converted to battery power requirement. These calculations include the efficiency drops across all the power generation and distribution components on the respective power paths.

This process is executed at each time step of the e-taxi, takeoff, and climb segments. At the end of each time step, the minimum SoC and the maximum current limits are checked. If either of the limits are violated, then the battery capacity must be increased. If neither of the limits are violated then there is room to decrease the capacity. Because changing the battery capacity means changing the battery weight and thus the aircraft takeoff gross weight, instead of stopping the mission analysis the discharge process automatically stops regardless of the pre-defined discharge schedule. The amount of additional required energy continues to be calculated based on the battery usage strategy. The total additional energy is calculated after the mission analysis is performed and used to size the battery. This approach reduces the number of iterations to fly the mission and size the aircraft and its propulsion system. The battery is sufficiently sized when one of the conditions given in Eq. (1) or Eq. (2) holds, where I is the battery current:

$$SoC = 20 \quad \& \quad I \leq I_{\max} \tag{1}$$

$$SoC \geq 20 \quad \& \quad I = I_{\max} \tag{2}$$

The case presented in Eq. (1) holds when the battery is sized based on the total energy requirement, whereas the case in

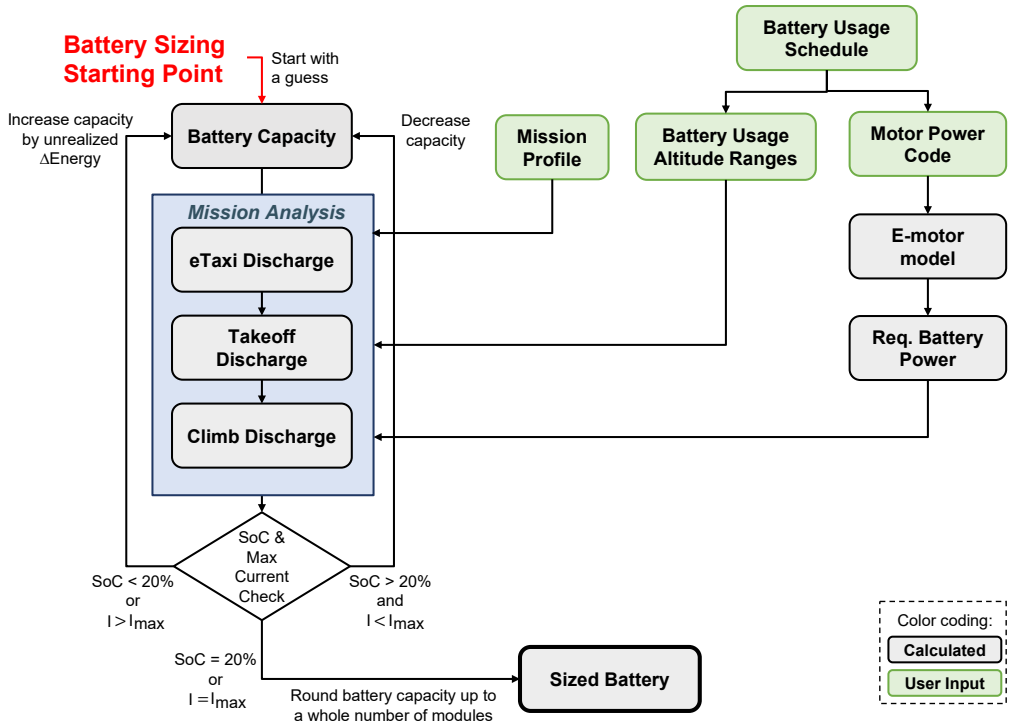

Fig. 12 Battery sizing process flowchart.

Eq. (2) holds when the battery is sized based on the maximum current (and thus power) draw at the cell level. The final capacity is obtained by rounding up the number of battery modules connected in series and parallel to integer values.

2. Power source sizing

The EAP vision vehicles maintain the power loading of the advanced turboprop vehicle. In each vehicle sizing iteration, the total power required is computed based on the current takeoff gross weight. A new term called the "electric motor power split" is defined as ratio of the maximum total power of the electric motors ($P_{EM,max,total}$) to the aircraft total sea level power ($P_{aircraft,SL,total}$), as given by Eq. (3). This term describes the level of hybridization of the parallel hybrid electric propulsion system at its sizing point. Note that the term "hybridization factor" is not used in exchange for the term "motor power split" here as it can create confusion between the power sizing points (which use a constant design factor) and the in-flight hybridization of the propulsion system (which varies throughout and across different flights).

$$PowerSplit = \frac{P_{EM,max,total}}{P_{aircraft,SL,total}} \tag{3}$$

Different motor power splits indicate different electric motor and engine sizes, and consequently different performance characteristics. Therefore, motor power split must be optimized for the desired system level performance.

The iterative power source sizing process which includes the co-sizing of the turboshaft engine and the electric motor is depicted in Fig. 13. The process takes in TOGW (guessed at the initial iteration) and a user-defined sea level

static power-to-weight ratio (P/W) for the entire aircraft to calculate the total sea level static power requirement. For the purposes of this study, the aircraft power-to-weight ratio and wing loading were matched to that of the baseline aircraft to approximately meet the same point-performance requirements. Then, the sea level engine rated power and maximum electric motor power are calculated by 3. Note that this approach is being improved in subsequent studies by including constraint diagram analysis within the aircraft sizing and synthesis loop [30].

In addition to the takeoff power requirement, the engine must meet the cruise ceiling power requirement at the cruise altitude. Some high motor power split values can result in a relatively small engine sea level static (SLS) takeoff power requirement which results in violation of the cruise ceiling power requirement. In such cases, the engine SLS power is increased to match satisfy the cruise ceiling power requirement.

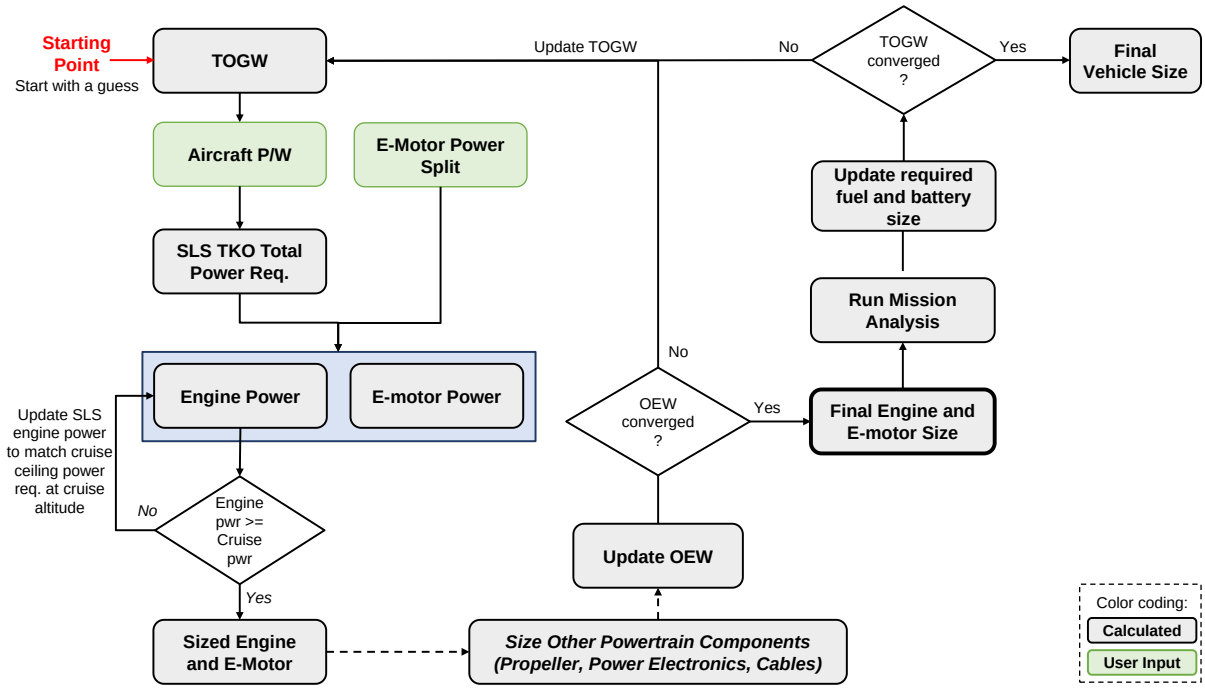

Fig. 13 Power source sizing process flowchart.

The engine and electric motor sizing process is followed by the sizing of all other powertrain components, such as the thrust source and power distribution elements. The powertrain weight manifests itself in operating empty weight (OEW), which triggers the first iteration loop. Iteration continues until OEW is converged. Then, the mission analysis is performed, the new energy source weights and the new TOGW are calculated. This triggers the second iteration loop which continues until the TOGW converges within a desired margin of error.

3. Thrust source sizing

For the 19-pax TRA, the 4-bladed propeller is resized by changing its blade profile, diameter, and design RPM within the range of Hamilton Standard maps [64] to achieve the highest average efficiency in the climb and cruise

segments of the primary mission.

For the 50-pax TRA, due to a lack of 6-bladed propeller performance maps, only the diameter and RPM is varied to meet the power requirement, while the dimensionless propeller performance characteristics (such as the advance ratio) are kept unchanged. Since the available power of electric motors does not vary with altitude and the available power of the advanced engines does not lapse as significantly as that of the baseline engines, propellers sized for sea-level takeoff could have their performance saturated as altitude increases before top-of-climb is reached. Therefore, the top-of-climb is selected as the sizing condition, and the propeller diameter is computed using Eq. (4) [65]:

$$D_{\text{prop}} = K_P \sqrt[4]{P_{\text{bhp}}} \tag{4}$$

where P_{bhp} is the total available shaft power at top-of-climb of all power sources connected to the propeller, and K_P is a coefficient determined from TRA model calibration.

D. Electrified Taxi Modeling

Taxi out and in were modeled as 10 and 5 minute idle mission segments, respectively, for the TRA and advanced vehicles. These idle mission segments are representative of steady-state taxi at a fixed thrust. Taxi out for the EAP vision system was modeled as a more detailed 10 minute taxi mission segment using a 2D physics model, with taxi in modeled as a 5 minute idle mission segment.

The EAP vision system taxi out mission segment is defined using a combination of steady-state taxi at a fixed thrust and acceleration requirements based on those identified by the Airbus Electric Green Taxiing System (EGTS) test program [66]. These acceleration requirements include runway crossing acceleration from 0 to 10 knots in 20 seconds at MTOW and taxiway acceleration from 0 to 18 knots in 90 seconds at MTOW. Taxi out was modeled as one runway crossing acceleration and two taxiway accelerations, where acceleration was assumed to be constant, with steady-state taxi for the remainder of the 10 minutes.

Thrust required during taxi out is calculated based on the rolling resistance and gravitational forces, as well as required acceleration. The rolling resistance is modeled using a breakaway resistance coefficient at 0 knots, which linearly transitions to a lower rolling resistance coefficient at 10 knots. The aircraft is assumed to be taxiing on an uphill 1.5% grade for the duration of taxi out, to account for a worse-case airport topography [67].

VI. Electrified Aircraft Design Space Exploration

The design space exploration and trade study investigates the EAP vision system's sensitivities to the modes of operation for the parallel hybrid electric architecture identified previously in Section V.A. In addition, the sensitivity of

the vehicle and mission level metrics of interest to select KPPs were also explored.

A. Electrified Aircraft Trade Study Setup

1. Design Space Definition

Prior to the trade study, three main questions were identified to define the right design space to thoroughly explore so that the optimum design maximizes the benefits electrification. These questions were: (i) *when*, (ii) *how much*, and (iii) *how long* electrification minimizes the fuel burn.

As discussed previously, the **electric motor power split** determines the ratio between the motor and engine size. At takeoff, both power sources provide maximum power. Thus, this variable describes *how much* power is required from each branch of the propulsion system.

The design space for the taxi segment is defined by a discrete design variable "**use e-taxi**." If it is set to "off", then the turboprops are used to taxi out. If it is set to "on", then only the electric motors provide the required power to taxi out ("*when*"). If the required taxi power is greater than the maximum electric motor power available, then e-taxi cannot be realized. **Taxi speed** and **taxi time** were also included in the design space as they directly impact the required motor size and the required battery capacity, respectively ("*how much*").

The battery usage schedule is an important factor that not only sizes the battery but also impacts the fuel burn benefits. The battery usage schedule during climb is represented by the following design variables: **Climb motor power code** describes *how much* thrust power is provided by the electric motor relative to its maximum power. Per the e-boost strategy, the engine always runs at its peak power setting.**Climb boost strategy** (discrete variable) describes *when* the electric motors are turned on and off (and when the battery is discharged) during climb. The "Low Altitude" setting indicates that climb e-boost starts right after the takeoff segment and continues until the specified altitude. "High Altitude" setting indicates that the motors are turned off after takeoff and turned on again at a specified altitude until the end of the climb segment (see Fig. 14). **Total boosting altitude** describes for *how long*, in terms of total altitude, the electric motors remained on during climb. It also specifies the start or end altitude for the climb boost strategy (see Fig. 14). The climb segment is modeled as a constant equivalent air speed climb to cruise altitude, as explained in Section III.A.1. The rate of climb is a fall-out parameter based on the thrust available and thus changes with climb boosting strategy.

During flight, the battery can be recharged during the cruise and/or descent segments. The flight segment during which the battery is charged (*when*) and the C-rate it is charged ("*how much*") at are defined by the "**cruise charging C-rate**" and "**descent charging C-rate**" design variables.

The remaining design variables include a select set of KPPs associated with the subsystem level design choices and technology levels. The complete set of design variables and ranges selected for this preliminary phase of the project are listed in Table 9.

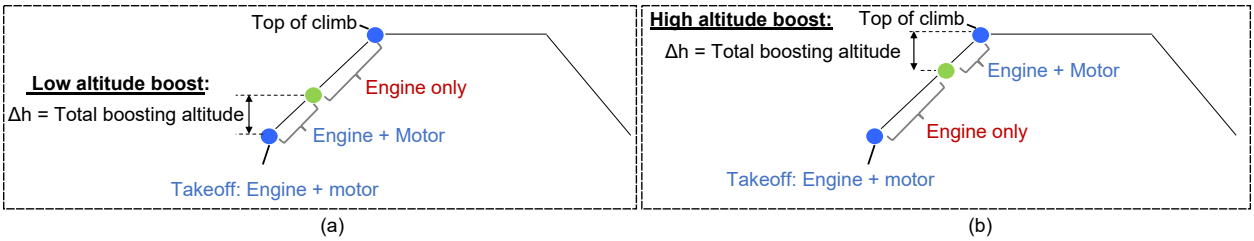

Fig. 14 Climb e-boost strategy and total power boosting altitude for (a) Low altitude boost, and (b) High altitude boost cases.

Table 9 Design space definition. Variables with asterisk are two-factor discrete variables. All others are continuous variables.

Design Variable	Minimum value	Maximum value
Electric motor power split	0	0.25
Climb boost strategy*	Low Altitude	High Altitude
Total boosting altitude	Sea level	Cruise altitude
Cruise charging C-rate	0	1.5
Descent charging C-rate	0	1.5
Use e-taxi*	Off	On
Steady taxi speed	18 kts	30 kts
Taxi time	5 min	10 min
System voltage	540 V	1260 V
Number of battery cells connected in series per module	3	16
Number of battery cells connected in parallel per module	2	11
Cable wire diameter	20 mm	50 mm
Power converter specific power	5 kW/kg	50 kW/kg
Electric motor specific power	3 kW/kg	30 kW/kg
Battery cell level specific energy	0.25 kWh/kg	1 kWh/kg
Battery pack scaling factor	0.25	1

2. Design of Experiments and Surrogate Modeling

Even if all the variables listed in Table 9 are evaluated at low, medium, and high settings while the binary variables are restricted to 2 settings, the design space would include $2^2 \times 3^{14} = 19\,131\,876$ combinations. On average, the sizing algorithm takes around 80-120 seconds per case on a computer with an Intel Core i7-8700 CPU at 3.2GhZ and a 16 GB RAM. This makes the complete evaluation of such a simple combination of input space infeasible. To alleviate this problem, surrogate modeling is used to evaluate the design space in real time and to enable trade-studies. Thousands of latin-hypercube design of experiment (DoE) cases evaluated using the electrified model provide the data to which surrogate models are fit. Two layer Artificial Neural Networks (ANNs) are found to provide training and validation errors of less than 1% within the three-sigma limits for most of the responses and are therefore used for the sensitivity analyses that follow. The battery state of charge is an exception with relatively higher error in its fits and is therefore

only used to understand the general trends.

B. Design Space Exploration and Sensitivity Analysis

A dynamic, interactive prediction profiler was built to visualize and explore the trends and tradeoffs among various factors for the responses of interest for each vehicle class. The profilers are powered by the ANN models. They demonstrate the isolated trends (partial derivatives) of each design factor to the responses of interest. Each point in the profiler corresponds to a sized vehicle. Thus, the visible trends and the overall aircraft design may dynamically change as a different value of a design factor is chosen.The profiler also provides a way to test the models by allowing counter-intuitive trends to be caught and investigated quickly.

The following two sections present different scenarios for the electrified 19 pax and 50 pax vision systems via static screenshots of the dynamic profilers. For these scenarios, the taxi out segment was assumed to be 10 minutes long with a steady taxi of 6.67 minutes at 18 kts. The battery cable length and cell density were also kept constant.

1. 50 pax profiler results

Figure 15 shows a specific configuration on a portion of the prediction profiler built for the 50 pax vision system. This configuration represents a conventional taxi operation scenario under the 2030 technology assumptions. The battery is not recharged during flight. Inspecting the trends in Fig. 15, the takeoff gross weight increases with increasing (electric) motor power split. This is mostly due to the battery weight contribution as the amount of required battery power and energy goes up with increasing motor power. The engine SLS rated power changes its downwards trend with increasing motor power split at around 18% split. This point of change represents the threshold at which the engine is sized by the cruise power requirement rather than the sea level takeoff power requirement. The cruise average BSFC follows a roughly inverse trend of the engine SLS rated power with the power split. This is due to the fact that in the turboshaft model built and used for this work, the engine becomes more efficient as the core gets bigger. The minimum block fuel burn is found at around 8% motor power split and 1250 volts of system voltage. The electric motors operate at maximum power during takeoff and climb.

It can be seen in Fig. 15 that charging the battery during cruise and/or descent increases the block fuel significantly. Descent charging C-rate seems to have a higher impact on fuel burn than cruise. Also, for this mission, the descent segment generally requires a higher C-rate to fully charge the battery than cruise due to having shorter time available to charge the battery.

Figure 16 shows the trade space for Scenario II – the same conventional taxi conditions, but this time the battery is fully charged at 0.25C during cruise. Comparing Figs. 15 and 16, a significant change in trends is seen due to charging the battery in flight. The minimum block fuel bucket seen at 8% motor power split in Fig. 15 has vanished in Fig. 16. After full power at takeoff, the electric motors are only used for the initial 2500 ft of climb at 25% of their maximum

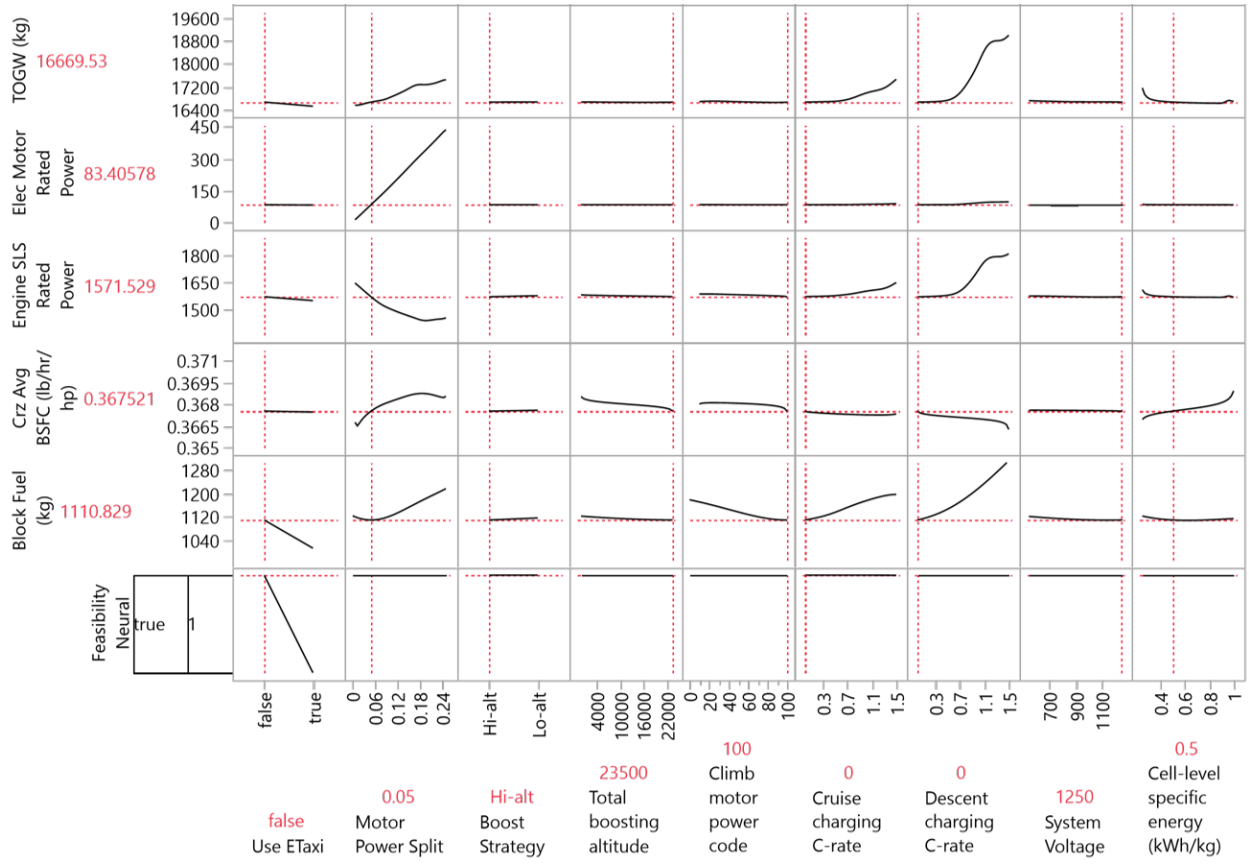

Fig. 15 50pax Scenario I: conventional taxi without in-flight battery charging.

power. Thus, the trends favor less electrification to reduce the block fuel burn. Nevertheless, at the design configurations given in Fig. 16, the ANN models predict a lower block fuel than the conventional 2030 advanced 50 pax model, however the predictions must be validated by running the same conditions in E-PASS. Charging the battery during cruise at 0.25C increases the block fuel burn prediction by about 2.5% compared to no in-flight charging presented in the previous scenario. Without any cruise charging, the battery must be charged at 0.9C during descent to achieve 100% SoC at the bottom of descent. This results in an increase of about 4% in block fuel burn compared to no in-flight charging. Note that Fig. 16 shows a strong trend in favor of e-taxi to minimize the block fuel burn.

Scenario III simulates the sizing trends where the taxi out segment is driven electrically. This scenario is given by Figure 17, where the "Use ETaxi" design factor is turned on. The minimum motor power required to taxi is determined by the probability curve called "Feasibility", generated from a binary ANN model, at the lower left corner of the profiler. To realize e-taxi, the motor power split (hence the electric motor size) must be chosen such that the probability of a successful e-taxi is predicted as 1 (100%). In the conditions given in Fig. 17, this minimum motor power split is around 13–14%.

In Scenario III, the battery is charged during flight. Utilizing e-taxi creates a minimum block fuel bucket in the

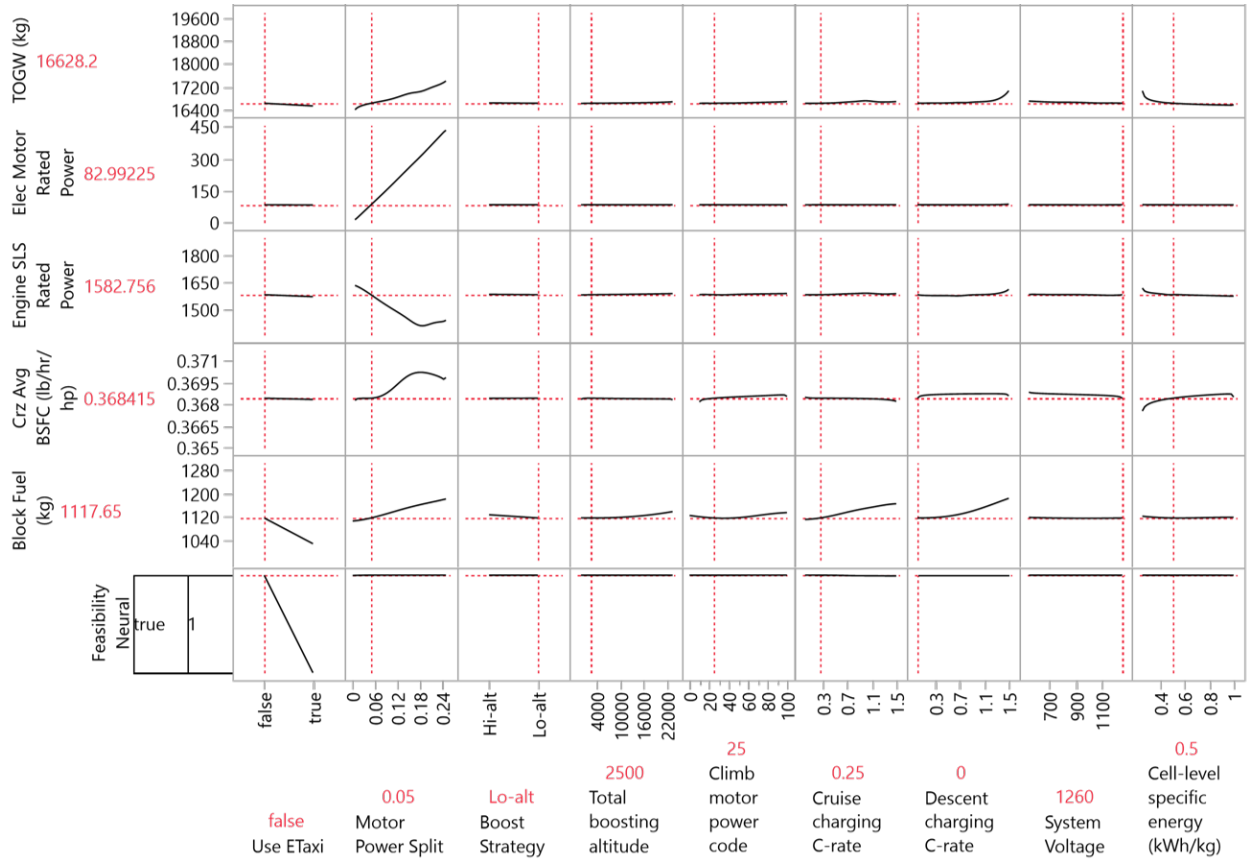

Fig. 16 50pax Scenario II: conventional taxi with in-flight battery charging.

motor power split trend, and provides significant fuel burn savings compared to Scenario II (conventional taxi). The minimum block fuel is achieved at 14% power split where the electric motors provide maximum power at takeoff and during the initial 12 000 ft of climb. The battery is charged at 0.4C during cruise. The block fuel vs. cruise and descent charging C-rate trends show that further fuel burn savings could be achieved without in-flight charging.

The reason why e-taxi provides additional fuel burn savings is that it does not necessarily require a larger battery. In some cases, the maximum power (i.e. max current) requirement is more stringent than the energy requirement, and even though a smaller battery could have provided the required energy, a larger battery is needed to provide the required power, as explained in the battery sizing strategy in Section V.C.1. In such cases, there is more energy stored in the battery than needed for the rest of the segments. As a result, e-taxi can leverage this excess energy that would otherwise remain in the battery. This is depicted in Fig. 18 where the battery SoC and fuel burn is shown as a function of mission time for no-e-taxi and e-taxi cases. The taxi segment covers the initial 10 minutes. In the case of e-taxi, the battery provides the energy required to taxi and SoC drops; whereas in the no-e-taxi case fuel is burned and battery is not used during taxi. The battery is used during takeoff and climb at the same rate in both cases, and not used in cruise. For the case of e-taxi, the battery SoC at the top of climb is lower than that of the no-e-taxi case (while respecting the 20%

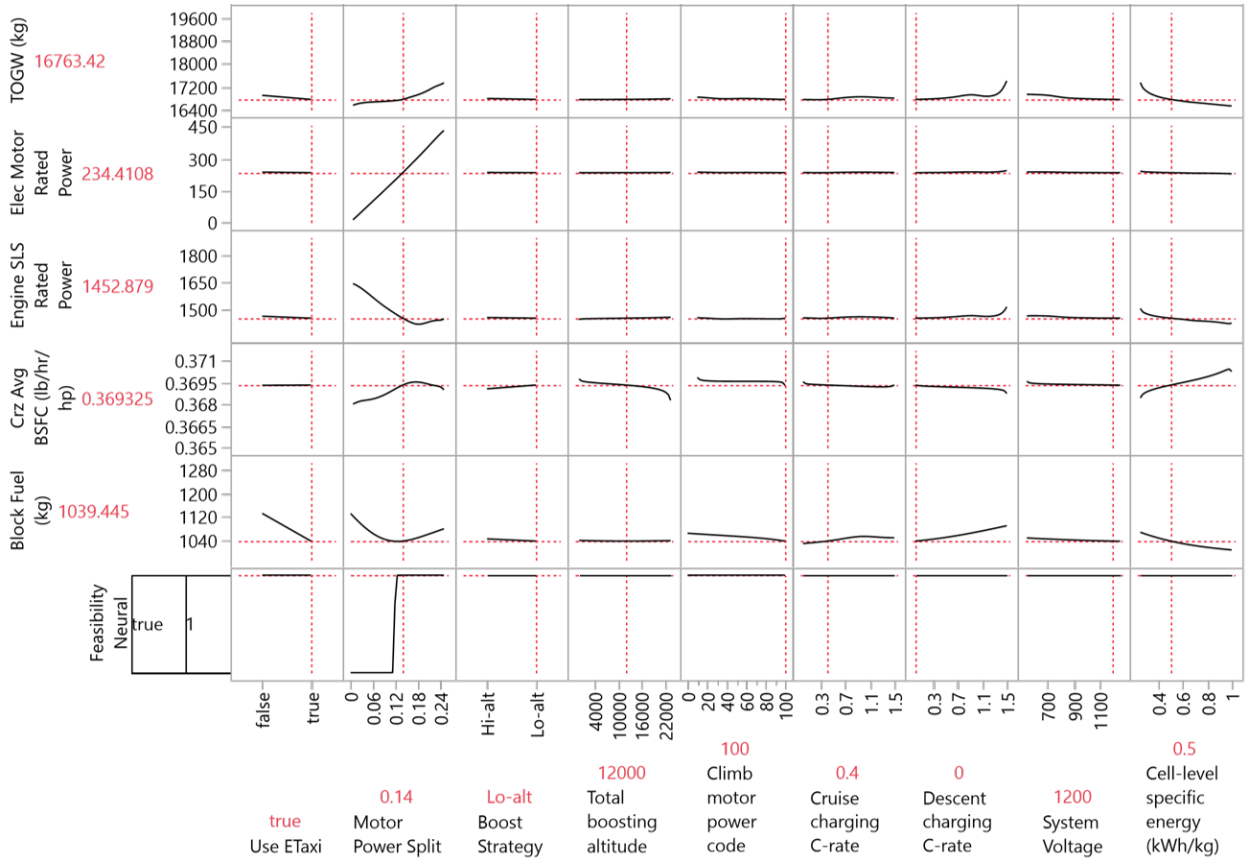

Fig. 17 50pax Scenario III: e-taxi with in-flight battery charging.

minimum SoC limit), and thus, the fuel burn is lower. Note that the e-taxi battery energy and power requirements were considered in the aircraft sizing process, and thus all of the points given in Fig. 17 are feasible as long as the the motor power split is at or above the minimum taxi-power requirement (as depicted by the "Feasibility" response).

Finally, Scenario IV investigates the sizing trends with e-taxi but without any in-flight battery charging, as shown in Fig. 19. As expected, the block fuel is the lowest among the four scenarios, thanks to the fuel saving effects of e-taxi and no battery charging during flight. Compared to Scenario III, Scenario IV favors using e-boost throughout the entire climb segment at full motor power. The motor power split trends does not show a significant change. Consequently, electrification is the most beneficial when the taxi out segment is fully electric, takeoff and climb power are fully boosted with the electric motors, and battery is charged on the ground as opposed to during flight. Also, note that while the block fuel trends favor ground charging, the actual cost of energy and CO_2 emissions due to charging the battery on the ground depends on the local power grid composition, and thus would vary among different airports [68].

2. 19 pax profiler results

Figure 20 shows a specific configuration on a portion of the prediction profiler built for the 19 pax vision system. Similar to the 50pax Scenario I (Fig. 15), this scenario assumes conventional taxi, 2030 technology levels, and no

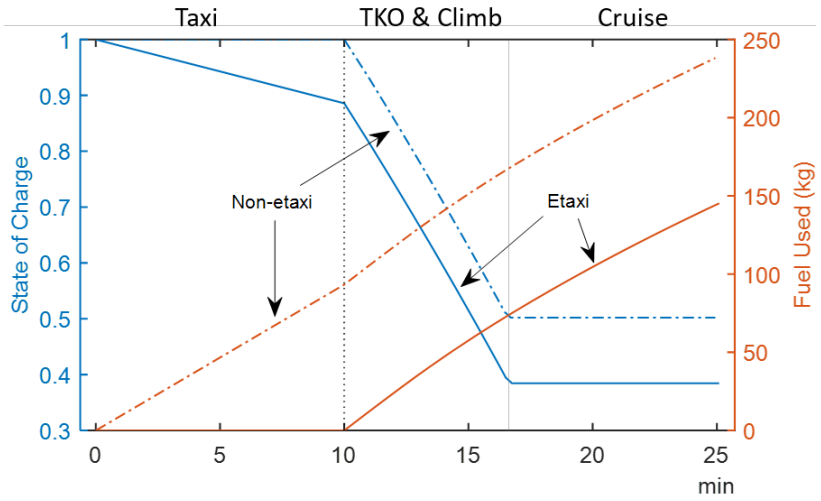

Fig. 18 Battery state of charge and fuel burn comparison for no e-taxi and e-taxi cases. For both cases, the battery is used during takeoff and climb at the same rates.

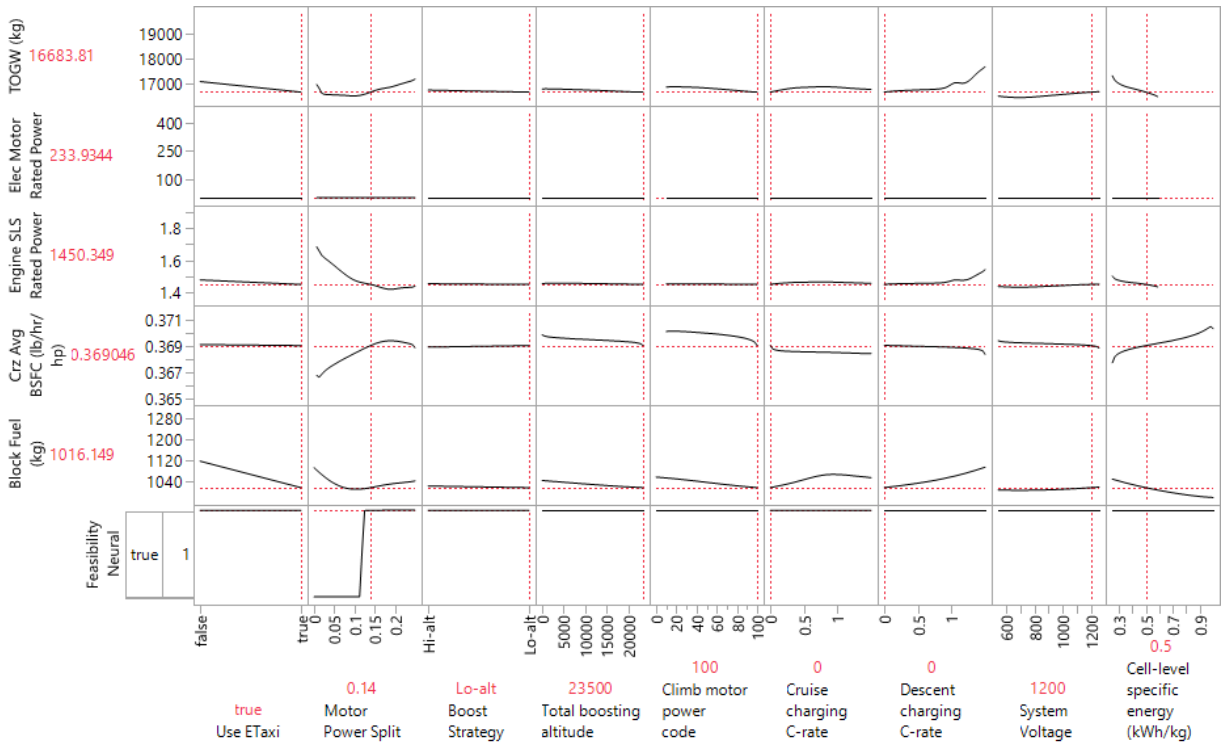

Fig. 19 50pax Scenario IV: e-taxi without in-flight battery charging.

in-flight battery charging. Unlike the 50 pax under the same scenario, the 19 pax trends favor the highest electrification within the design variable ranges. The maximum fuel burn benefits are obtained at the maximum electric motor power split of 25%, where the electric motors provide maximum power during takeoff and climb. Variation in system voltage does not make any significant impact on the predicted responses. Similar to the 50pax, in-flight battery charging during cruise or climb significantly increases the block fuel predictions.

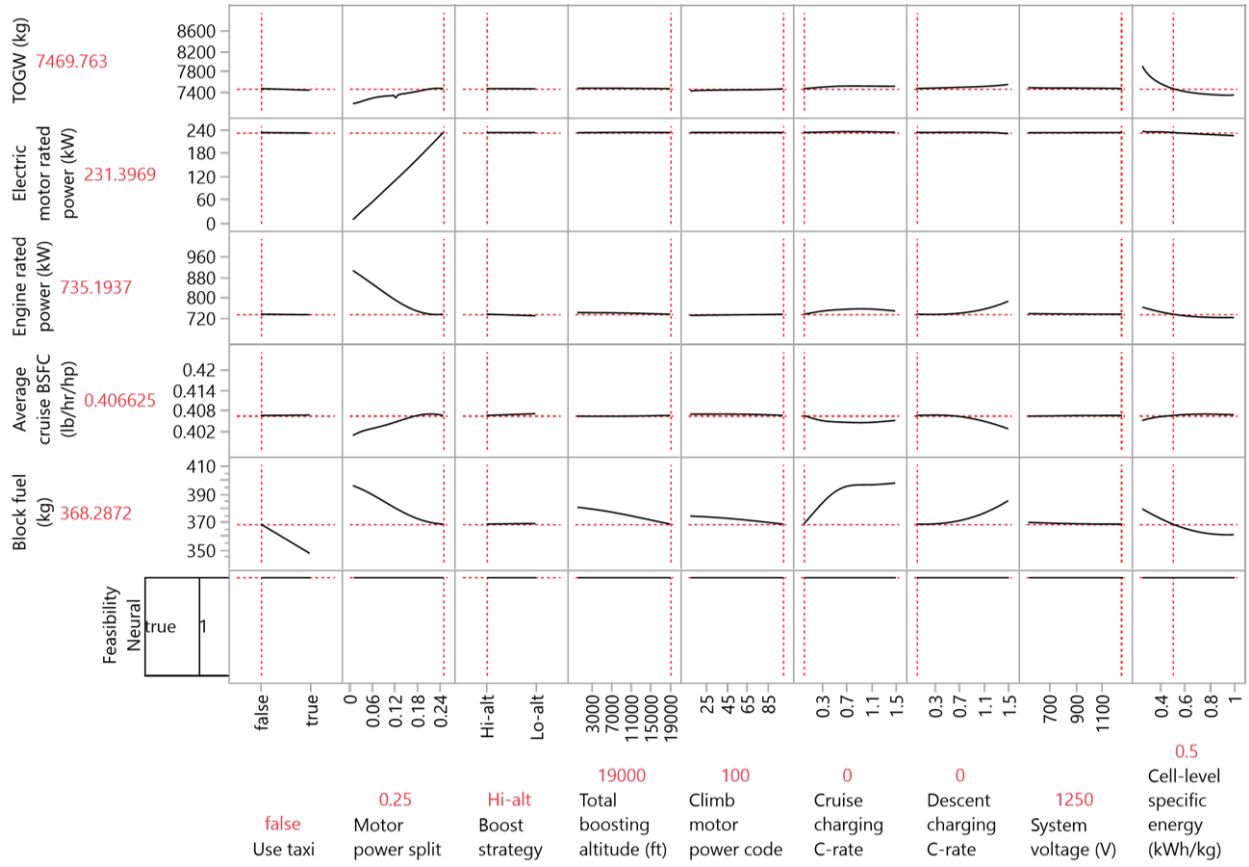

Fig. 20 19pax Scenario I: conventional taxi without in-flight battery charging.

Figure 21 reflects Scenario II where the battery is charged at 0.6C during cruise. The block fuel - motor power split trend is somewhat inverse of that of seen in Scenario I in Fig. 20, and the minimum block fuel burn solution shifts to the minimum electric motor power split. The minimum block fuel bucket seen in the cruise charging C-rate plot can be interpreted as a sign of the tradeoff between requiring more engine power to charge the battery at high C-rates and reaching the 100% SoC target sooner in cruise. Note that once the battery is fully charged, the charging stops immediately, and the battery is not charged beyond 100% SoC regardless of the input charging C-rate value. Additionally, charging impacts the block fuel – system voltage trend, making lower system voltages more favorable compared to Scenario I. This is likely due to the configuration for the series and parallel cells selected behind the scenes to achieve minimum block fuel. The full trends, including the cell configurations, are provided in the appendix of this

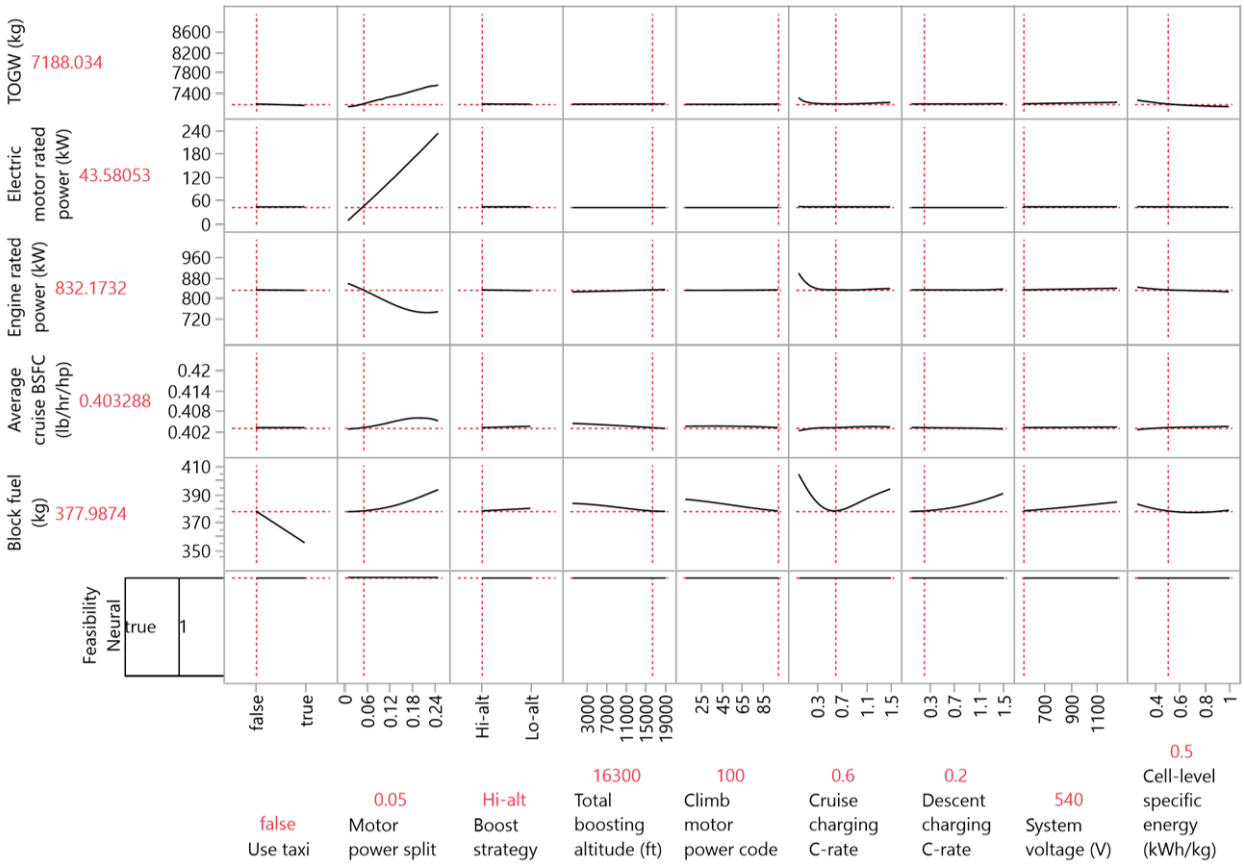

Fig. 21 19pax Scenario II: conventional taxi with in-flight battery charging.

paper.

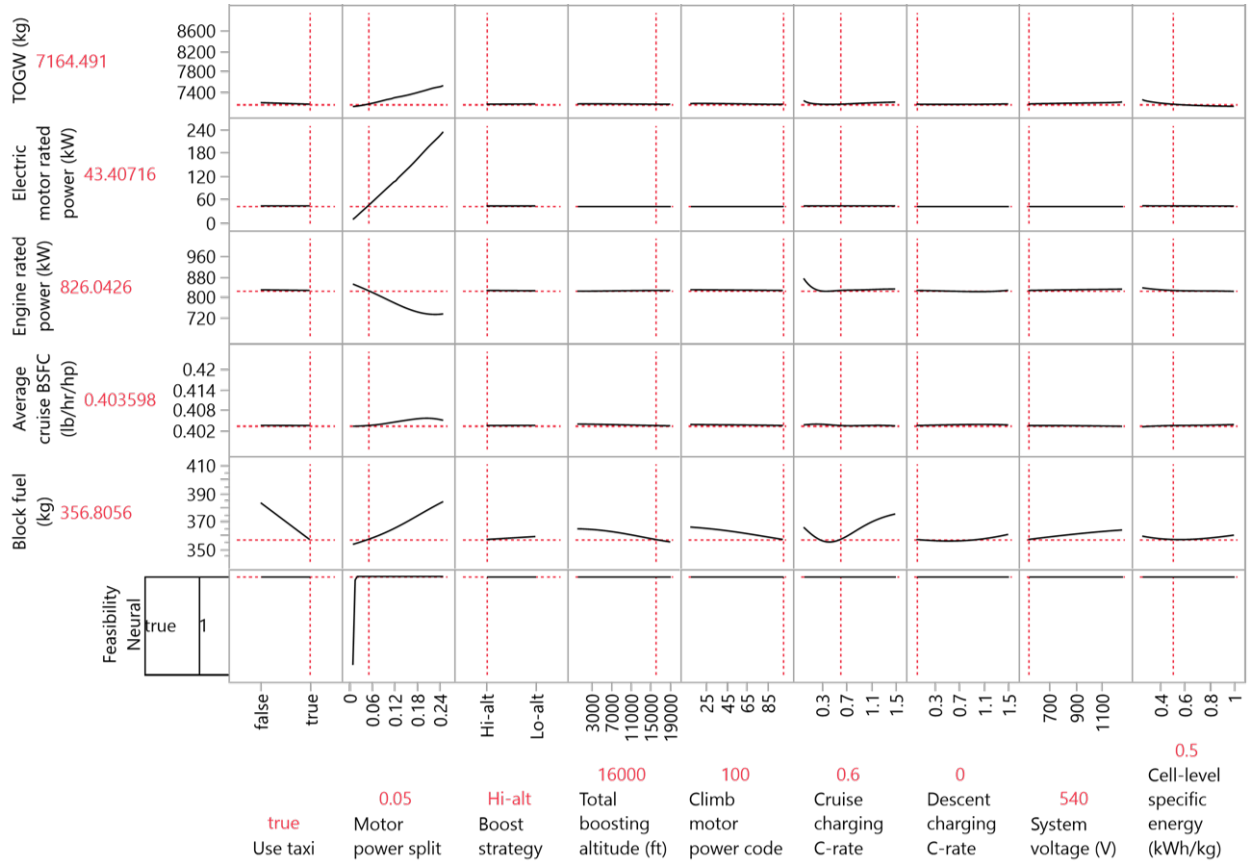

Fig. 22 19pax Scenario III: e-taxi with in-flight battery charging.

Similar to the 50pax trade space, electric taxi provides significant block fuel benefits for this class of EAP vehicles. 19 pax Scenario III given in Fig. 22 includes e-taxi and in-flight battery charging at 2030 EAP technology levels. Compared to Scenario II, the optimum sizing point changes slightly due to e-taxi. A 5% motor power split enables the e-taxi operation. The electric motors provide maximum power during takeoff and the final 16,000 ft of climb. The battery is charged at 0.6C during cruise. This optimized vehicle design with e-taxi is predicted to provide more than 5% block fuel burn savings compared to the optimum vehicle design without e-taxi.

Finally, Scenario IV given in Fig. 23 includes e-taxi but does not include in-flight battery charging. Similar to the trends observed for the 50 pax vehicle, e-taxi combined with full takeoff and climb e-boost where the battery is charged only in the ground is the best scenario for EAP in terms of minimizing the block fuel burn. Note that in both Scenario I and Scenario IV (Figs. 20 and 23) where there is no in-flight charging, the block fuel trends favor the highest motor split, i.e. the largest possible electric motor, whereas Scenarios II and III (Figs. 21 and 22) with in-flight battery charging sees a block fuel penalty at higher motor power split settings. This is due to the fact that more battery energy is needed to run a larger electric motor, and more fuel is needed to fully charge the battery during flight. The weight penalty due to the

larger battery is compensated by the benefits of e-taxi and e-boost, but not when jet fuel is used to charge the battery in-flight.

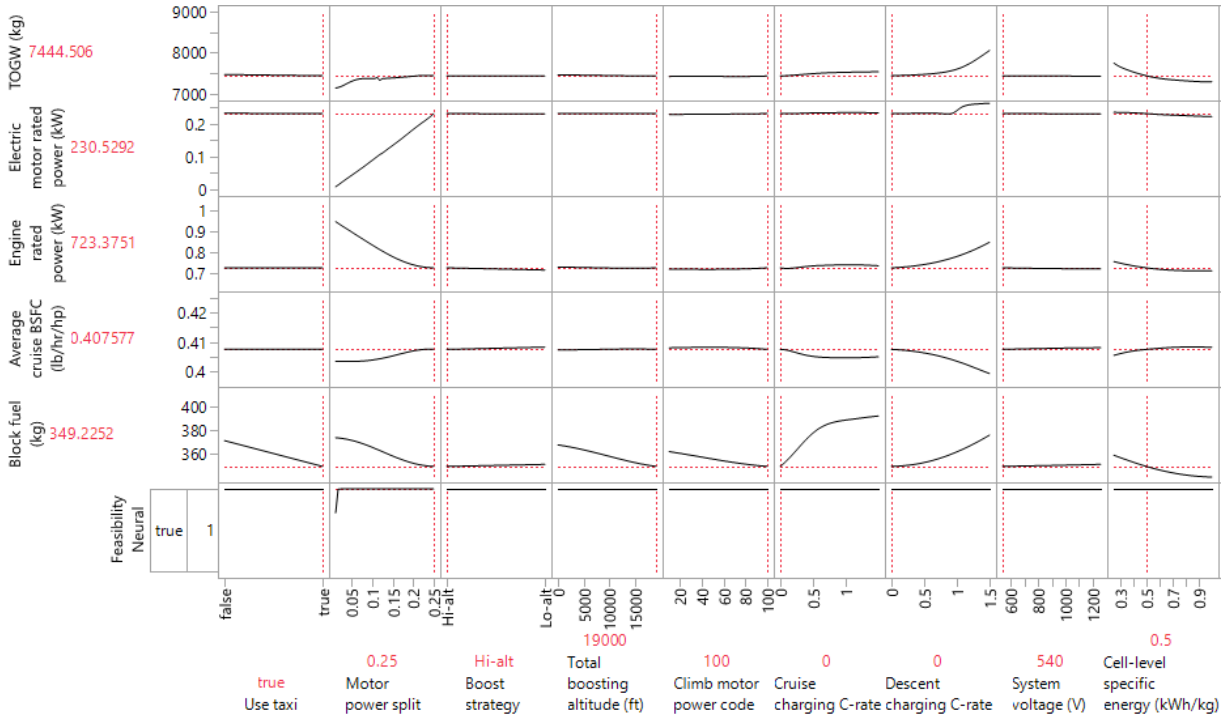

Fig. 23 19pax Scenario IV: e-taxi without in-flight battery charging.

Figures 15- 23 show the trends for the chosen settings. A change in a single design variable can impact the shape and direction of these trends, shifting the optimum design point to different settings in the rest of the design variables. The authors gave an example of this dynamic nature of the multi-dimension trade space by going through four important scenarios per vehicle, however there are countless other that can be explored by these dynamic profilers.

This section provided a subset of the results obtained by the design space exploration study. Further results including the full list of design variables and some additional responses of interest are provided in the Appendix of this paper. Isolated trends for climb power boosting, in-flight charging, and e-taxi for the 50-pax aircraft have been published in Ref. [32].

C. EAP Vehicle Results

The prediction profilers shown and discussed in Section VI.B were used to explore the complex trade space of thousands of electrified aircraft designs. However, the surrogate modeling introduces some level of prediction error in exchange for computational speed. Thus, the minimized block fuel sizing points chosen using the prediction profilers were validated by running the design variable settings in E-PASS to remove any prediction errors.

The trade space exploration study revealed that e-taxi can be crucial for block fuel burn reduction. Moreover,

in-flight battery charging can diminish the benefits, and there is a complex tradeoff between the rate of charge and additional block fuel consumption due to charging.

Tables 10 and 11 provide a summary of the results of Scenarios I through and IV (S.I through S.IV) against the 2030 Advanced Vehicle with the conventional propulsion system (designated as Scenario 0, or S.0) for the 50 and 19 passenger classes, respectively. The advanced conventional and the electrified aircraft share the same 2030 technologies in terms of the turbomachinery, aerodynamics, and structures. Thus, the deviations in S.I-IV vehicles are caused by optimization of the vehicle design and operation for the chosen electrification scenario.

Table 10 Sensitivity analysis results for the 50 pax. Electrified power management strategies are as follows: S.I: 5% motor power split, full power at takeoff, full climb e-boost at full power. S.II: 5% motor power split, full power at takeoff, low altitude climb e-boost at 25% motor power for 2500 ft. S.III: 14% motor power split, full power at takeoff, low altitude climb e-boost at full motor power for 12000 ft. S.IV: 14% motor power split, full power at takeoff, full climb e-boost at full power.

Scenario	Block fuel (kg)	Cruise avg BSFC (lb/hr/hp)	Engine SLS rated power (kW)	Electric motor rated power (kW)	Battery capacity (kWh)	OEW (kg)	TOGW (kg)
S.0 - Advanced Conventional	1165	0.3679	1657	N/A	N/A	10419	16539
S.I - EAP no e-taxi; no charging	1151	0.3684	1598	84	75	10494	16778
comparison over S.0	*-1.17%*	*+0.13%*	*-3.61%*	-	-	*+0.72%*	*+1.45%*
S.II - EAP no e-taxi; battery charged	1150	0.3687	1586	83.4	37.8	10463	16657
comparison over S.0	*-1.29%*	*+0.22%*	*-4.28%*	-	-	*+0.42%*	*+0.71%*
S.III - EAP with e-taxi; battery charged	1074	0.3697	1456	237.0	133.2	10542	16895
comparison over S.0	*-7.81%*	*+0.49%*	*-12.13%*	-	-	*+1.18%*	*+2.15%*
S.IV - EAP with e-taxi; no charging	1055	0.3700	1476	240.3	205.2	10612	17127
comparison over S.0	*-9.37%*	*+0.58%*	*-10.92%*	-	-	*+1.86%*	*+3.55%*

Table 11 Sensitivity analysis results for the 19 pax. Electrified power management strategies are as follows: S.I: 25% motor power split, full power at takeoff, full climb e-boost at full power. S.II: 5% motor power split, full power at takeoff, high altitude climb e-boost at full power for 16300 ft. S.III: 5% motor power split, full power at takeoff, high altitude climb e-boost at full power for 16000 ft. S.IV: 25% motor power split, full power at takeoff, full climb e-boost at full power.

Scenario	Block fuel (kg)	Cruise avg BSFC (lb/hr/hp)	Engine SLS rated power (kW)	Electric motor rated power (kW)	Battery capacity (kWh)	OEW (kg)	TOGW (kg)
S.0 - Advanced Conventional	385	0.4046	866	N/A	N/A	4527	7133
S.I - EAP no e-taxi; no charging	386	0.4048	772	232	131	4687	7636
comparison over S.0	*+0.42%*	*+0.05%*	*-10.89%*	-	-	*+3.55%*	*+7.05%*
S.II - EAP no e-taxi; battery charged	388	0.4037	835	43.9	32.4	4556	7240
comparison over S.0	*+0.78%*	*-0.22%*	*-3.58%*	-	-	*+0.64%*	*+1.50%*
S.III - EAP with e-taxi; battery charged	363	0.4036	829	44	25.9	4539	7183
comparison over S.0	*-5.71%*	*-0.25%*	*-4.27%*	-	-	*+0.27%*	*+0.70%*
S.IV - EAP with e-taxi; no charging	361	0.4049	769	230	120	4688	7587
comparison over S.0	*-6.15%*	*+0.06%*	*-11.14%*	-	-	*+3.57%*	*+6.37%*

Comparing the predicted responses shown in Figs. 15-19 against S.I-S.IV results in Table 10 shows that the

ANN models under-predicted the responses by a small margin (highest error under 3.9%). Compared to the advance conventional aircraft (S.0), both electrified 50 pax aircraft with conventional taxi can achieve almost the same fuel burn savings. However, this is only because a much smaller portion of the climb segment is electrified in S.II and the battery is almost half the size compared to the battery in S.I. Thus, ground charging allows more electrification, but a fully electrified climb segment comes with a bigger battery and takeoff gross weight penalty. In both cases, the turboshaft engine is slightly smaller than S.0, and the cruise average shaft power specific fuel consumption increases marginally.

As the ANN models predicted, taxiing with the battery and the electric motors provide significant block fuel burn benefits. The electrified 50 pax aircraft with e-taxi (S.III) provides 7.81% block fuel savings compared to the advanced conventional system. It requires a bigger electric motor to enable e-taxi, but also a much smaller turboshaft engine. The overall energy hybridization is higher than the vehicle optimized for S.II. The bigger and heavier battery drives the takeoff gross weight higher by 2.15% compared to the advanced conventional baseline. Finally, the maximum block fuel savings of 9.37% is obtained in S.IV where the battery is not charged during flight. The fuel savings come in spite of electrifying the entire climb segment at full power. As a result, S.IV employs a battery that has a capacity of about 1.54 times larger than that of S.III. S.IV has also the heaviest takeoff gross weight of all scenarios. Despite being the heaviest and largest aircraft, S.IV has the best electrification and power management strategy that brings significant fuel burn savings.

Similar results were obtained for the 19 pax EAP vehicles. Comparing Figs. 21 and 22 against S.II and S.III results in Table 11 shows that the ANN models created for the 19 pax vehicle under-predicted the responses of interest by a small margin (highest error around 2.6%). At the assumed cell-level battery specific energy of 500 Wh/kg, neither of the 19 pax EAP with conventional taxi (S.I and S.II) shows fuel burn benefits over the advanced conventional baseline. In fact, both of them burn slightly more block fuel to fly the same mission due to the increased weight of the system. However, the utilization of e-taxi changes the results significantly. Under the same technology assumptions and a very similar hybridization strategy, the electrified 19 pax aircraft with e-taxi and in-flight charging (S.III) provides around 5.71% block fuel savings over the advanced conventional aircraft. This reduction in fuel weight had a snowball effect on system and battery weight, finally causing the takeoff gross weight to be lower and requiring a smaller battery with a similar power split and energy management strategy. Finally, the maximum benefits of electrification are obtained in S.IV where the aircraft taxis out electrically and the battery is charged on the ground. As was the case for 50 pax EAP, S.IV enjoys a full e-boost during the entire climb segment. Thus, it has a larger battery and heavier takeoff gross weight than S.0 and S.III, but brings significant fuel burn savings over the conventional propulsion system.

VII. Conclusion and Future Work

This paper explored the complex design space for thin-haul and regional class charge-depleting parallel hybrid electric aircraft. These classes were represented with a 19- and 50-passenger aircraft modeled based on publicly

available data on B1900D and ATR 42-600. Aircraft technologies predicted to be employed by 2030 EIS vehicles were identified. These technologies were captured as improvements in turbomachinery, aerodynamics, and structures dating from the original EIS of technology reference aircraft to the target EIS year of 2030. The selected technologies were infused into each model and both aircraft were sized for their respective point performance and mission requirements. The resulting 19- and 50-pax Advanced Technology Aircraft with conventional propulsion systems set a benchmark to compare the impact of electrification.

The parallel hybrid electric architecture was developed based on physics-based models within E-PASS. Several modes of operation were identified and applied parametrically. The parametric nature of the models and the modes of operation sets this study apart from the others, as it enables a thorough investigation of a very complex, combinatorial design space for electrified aircraft. A design space exploration plan was laid carefully to answer three types of questions about electrification: *when*, *how much*, and *how long* should the propulsion system be electrified to minimize its block fuel burn. This approach revealed many design trends that were not explored before, such as low vs. high altitude climb e-boost. Furthermore, battery discharging and charging strategies were parametrically modeled, extending the battery-related design trades to all segments of flight. Taxi operations for each vehicle class were modeled in detail to allow for electric taxi modeling.

The resulting very large design space was represented by 16 design variables. A design of experiments was created for each vehicle class, and two layer ANNs were fit to the responses obtained from these experiments. This approach enabled real-time exploration of the design space and trade-studies. A subset of the results were presented in this paper under four different scenarios: conventional taxi with and without in-flight battery charging, and e-taxi with and without in-flight charging. These scenarios were chosen to be presented among many other trends discovered in this study due to the limiting nature of static screenshots from the dynamic prediction profilers developed for this purpose. The remaining trends and results will be published later on in subsequent papers.

The analyzed scenarios showed that in-flight battery charging during cruise and/or descent diminish the block fuel savings provided by EAP. In fact, the 19-pax EAP vehicle had a slightly higher block fuel burn than the conventional system when the battery was charged during flight. This result significantly changed when electric taxi operation was introduced to the EAP systems. E-taxi provided significant fuel burn benefits

Finally, in-flight charging limited the amount of electrification through the electric motor size and its operation during climb. However, when coupled with e-taxi, aircraft sized under the in-flight charging requirement still showed significant fuel burn benefits. This result is very promising. It proves the case for a parallel hybrid electric aircraft in thin-haul and regional markets, even if the ground charging infrastructure is not available at every airport by the target entry-into-service date of 2030-2035. If the batteries can be charged or swapped at the gate within a reasonable turnaround time, then a much higher degree of electrification can be achieved and the block fuel can be further reduced. Future work can include analysis on the life-cycle cost of CO_2 emissions due to charging the battery on the ground

compared to during flight.

This work revealed the potential impact of e-taxi on block fuel. Future work will repeat this study with improved propeller and taxi models. Moreover, it was discussed that for some cases, the battery was sized by the power (maximum discharge) requirement rather than the energy requirement. This means that a larger and heavier battery had to be employed and carried throughout the flight, and not all the energy in the battery was utilized during flight. In such cases, a smaller electric storage system could have been achieved by using a hybrid battery and ultracapacitor system where the ultracapacitor would carry the high power loads instead of the battery alone. Future work can test this hypothesis by modeling and analyzing such a hybrid energy storage system.

This work has focused on the early stage design space exploration and system-level analysis and tradeoffs of electrification. Such early stage analysis are crucial to understand the impact of revolutionary technologies on aircraft design and performance. Once the design space is well-understood and thoroughly analyzed, more detailed analyses must be carried out for later stages of conceptual design. For instance, the thin haul and regional aircraft analyzed in this study are particularly sensitive to weather conditions. Later stage analyses should include the effect of adverse weather operations on the resizing of components and systems. Moreover, once further details of the hybrid powertrain architecture are established, constraint analysis and failure scenarios (such as one-engine-inoperative) must be included in the aircraft sizing and synthesis process.

This paper lays a foundation for a series of subsequent publications. It describes the methodology developed to explore the complex design space opened by propulsion system electrification and presented the preliminary results for the sensitivity analysis of 19- and 50-pax 2030 vision systems for the NASA Electrified Powertrain Flight Demonstration program. The subsequent papers will improve the models and assumptions, explore other electrified propulsion system architectures (such as series hybrid) and the results will be updated and published accordingly. Future work will include a detailed thermal management modeling approach, and the impact of electrification of secondary subsystems.

Acknowledgments

This work has been sponsored by the NASA Aeronautics Research Mission Directorate and Electrified Powertrain Flight Demonstration project. The authors would like to thank the NASA EPFD project leadership Gaudy Bezos O'Connor and Ralph Jansen, and the EPFD project team for their technical guidance and valuable feedback. The authors also thank their project team members at Georgia Tech including: Dr. Jonathan Gladin, HyunKi Lee, Salah Tarazi, Blake Tiede, Christopher Hall, Dr. Cedric Justin, Dr. Evan Harrison, Dr. Joshua Brooks, and Vanessa Wu for their support in completing this phase of the work.

Appendix

This appendix provides screenshots from the full prediction profilers for the 19- and 50-pax vehicle trade space. Figures 24 and 25 are the two parts of the full profiler for 50-pax Scenario III with e-taxi and in-flight charging under 2030 technology assumptions. Figures 26 and 27 display the trends for a different design point for the same scenario assuming a 4% year over year improvement for 10 years (i.e. a factor of 1.04^{10} improvement) in cell-level specific energy, battery packaging weight scaling factor, and power converter and electric motor specific power. Finally, Fig. 28 and 29 provide the two parts of the full profiler for 19-pax Scenario III with e-taxi and in-flight charging under 2030 technology assumptions.

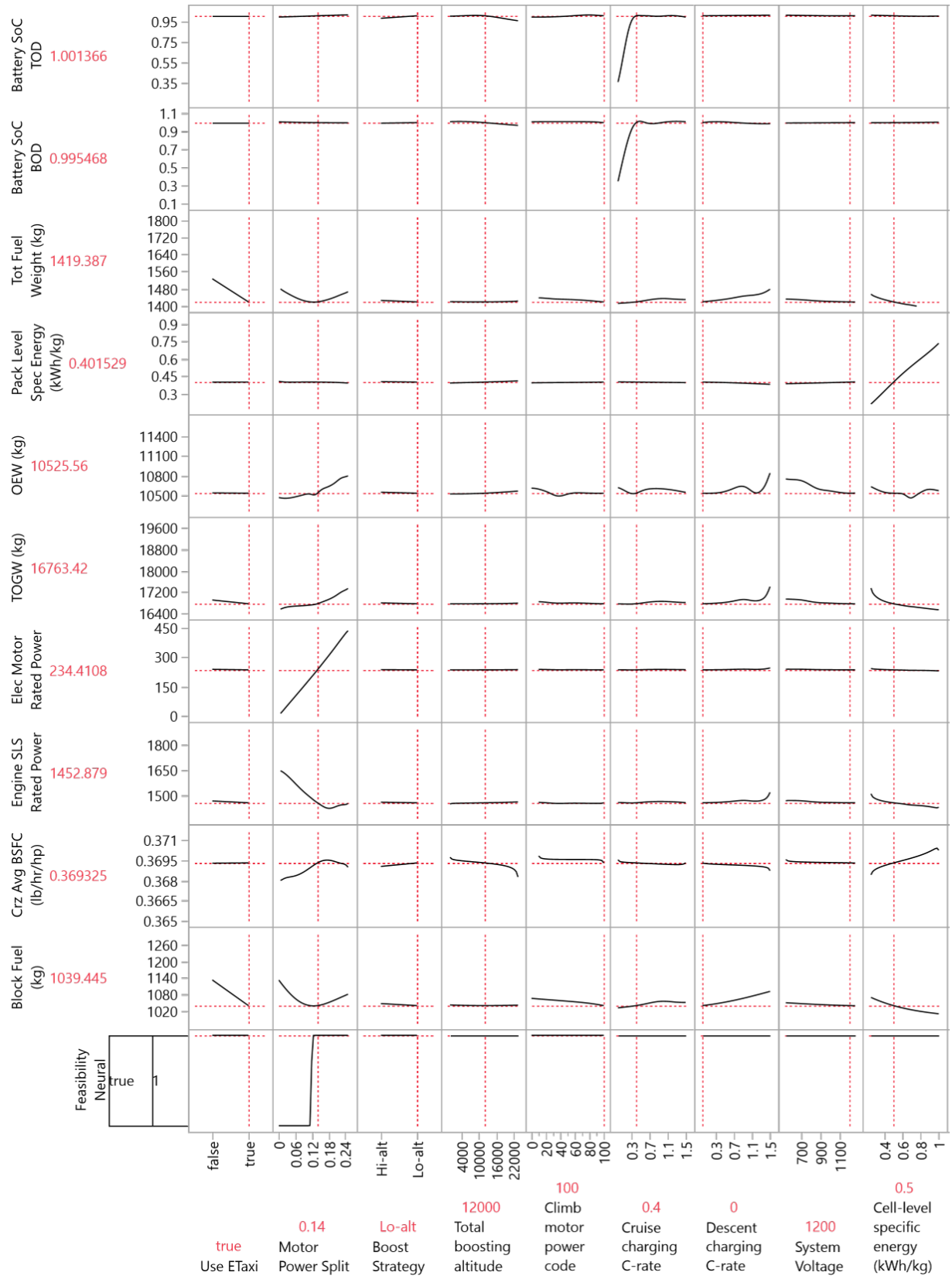

Fig. 24 Part 1 of the full profiler for 50-pax Scenario III with e-taxi and in-flight charging. 2030 technology assumptions.

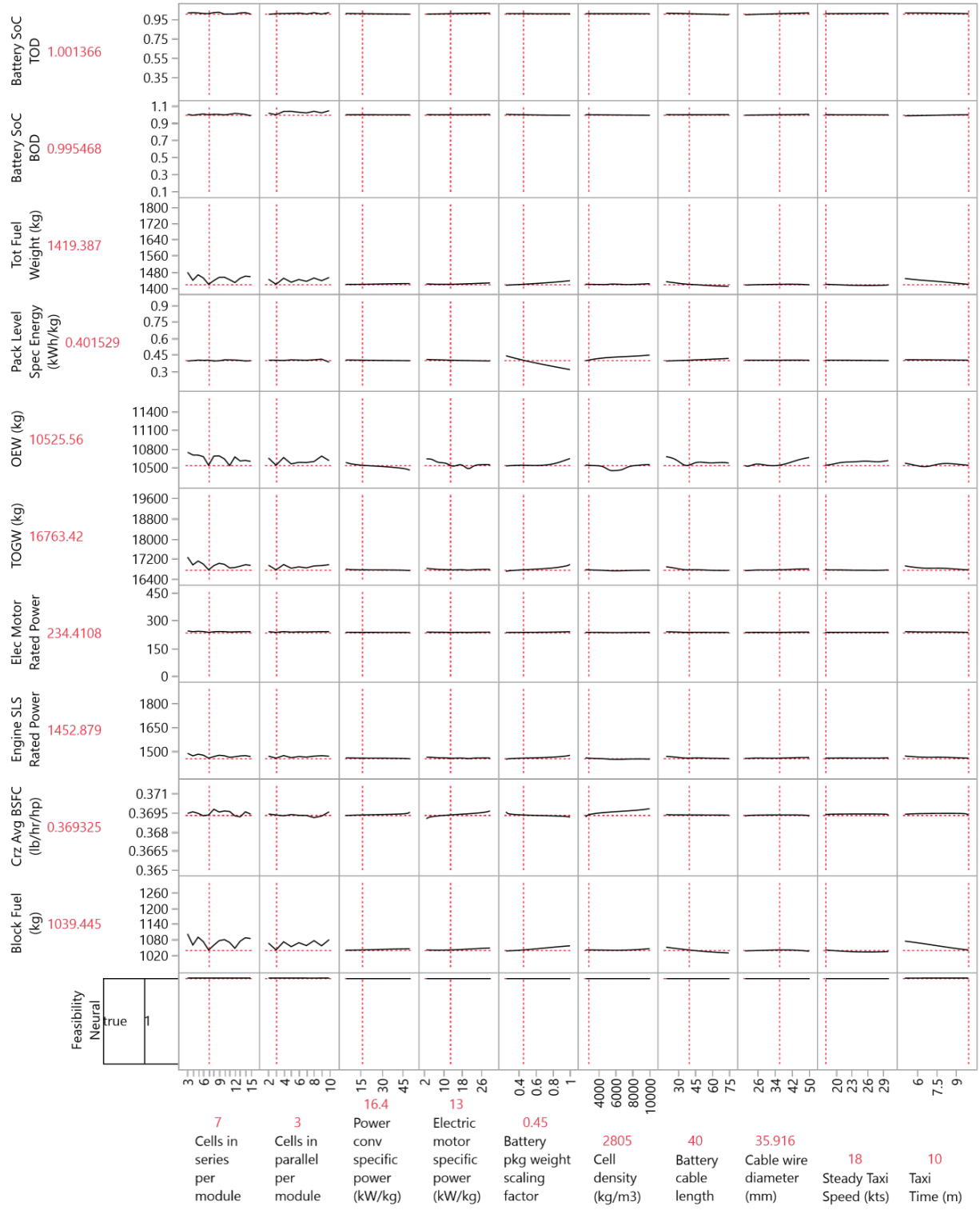

Fig. 25 Part 2 of the full profiler for 50-pax Scenario III with e-taxi and in-flight charging. 2030 technology assumptions.

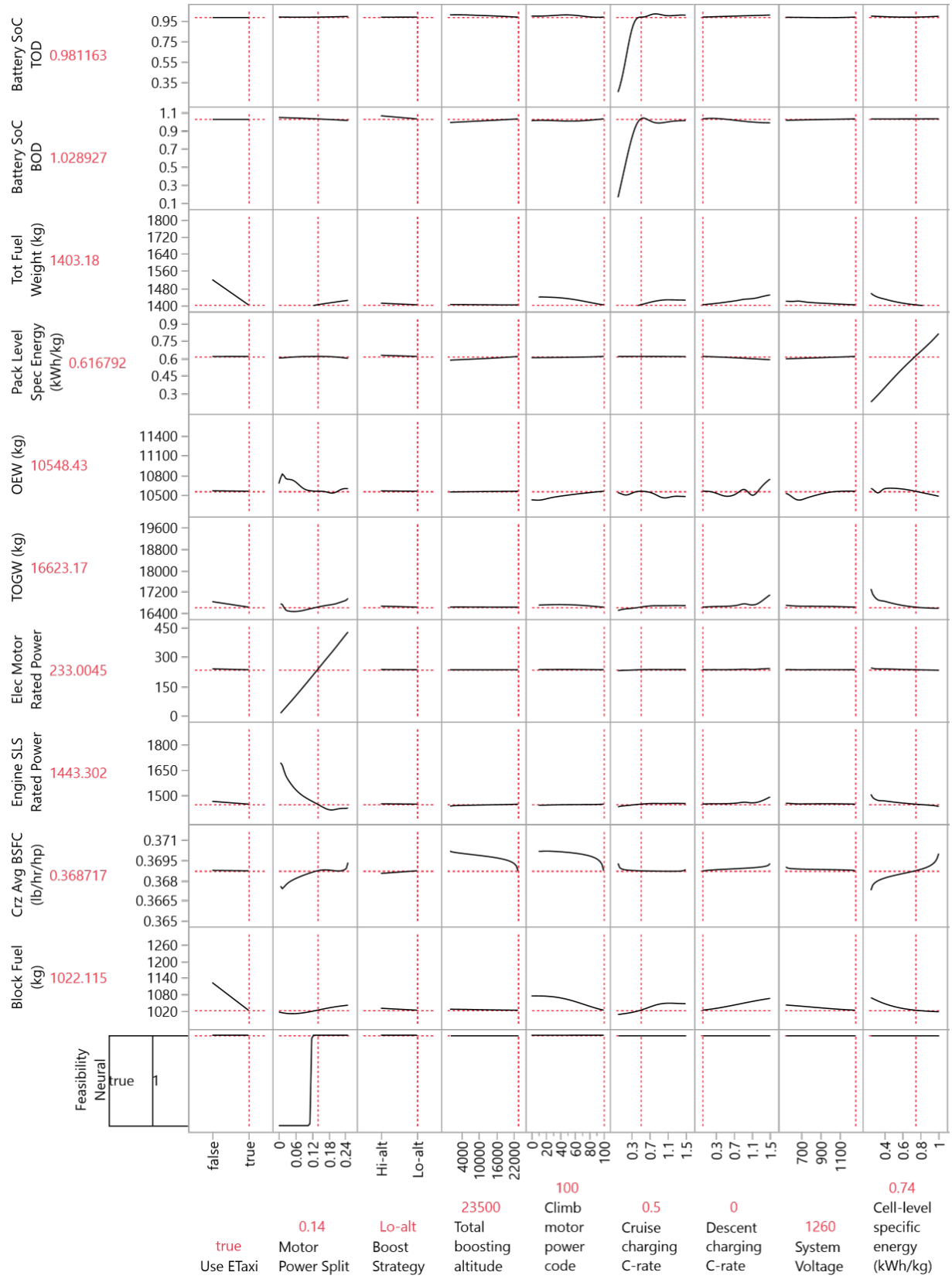

Fig. 26 Part 1 of the full profiler for a 50-pax design point with e-taxi and in-flight charging under improved technology levels.

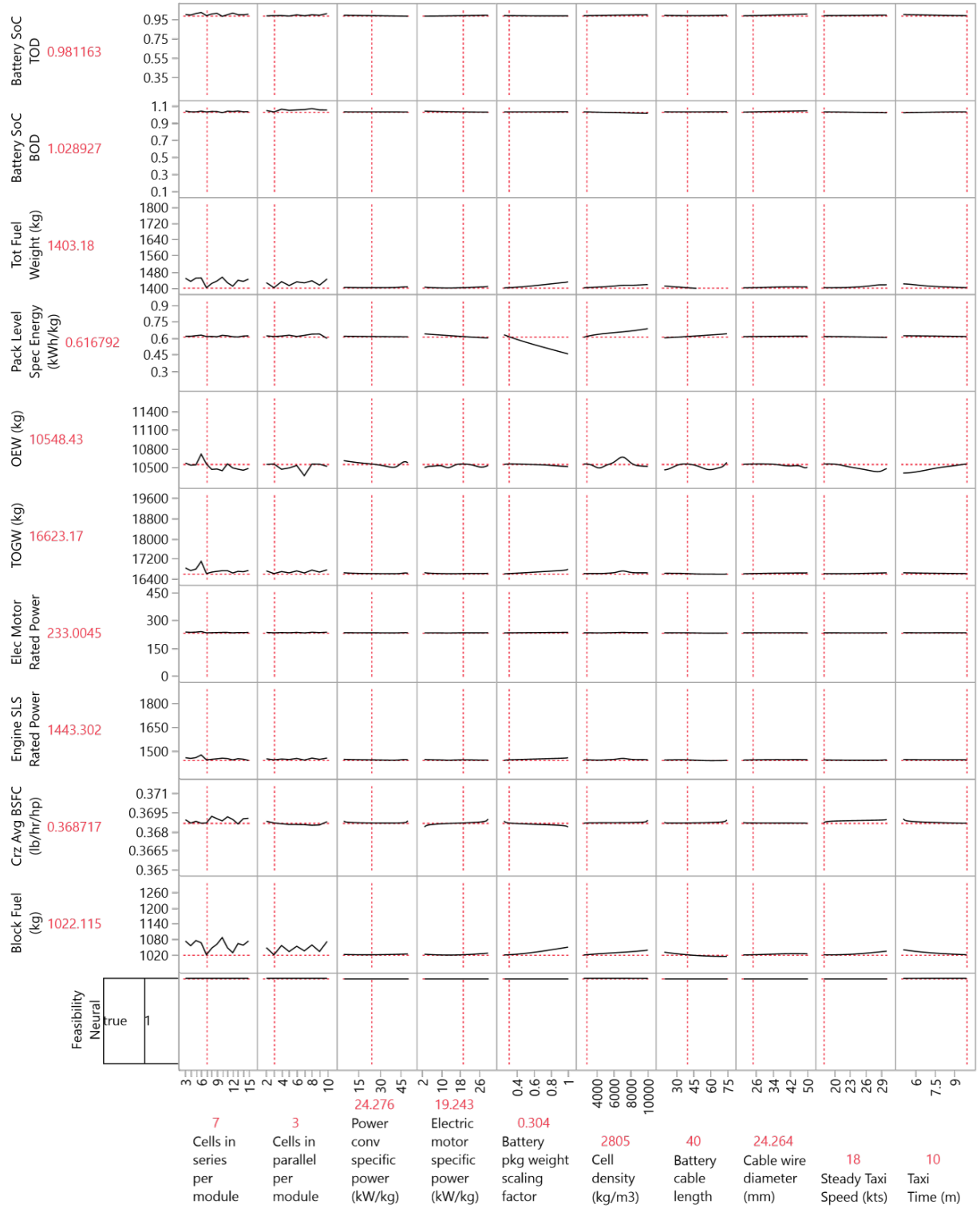

Fig. 27 Part 2 of the full profiler for a 50-pax design point with e-taxi and in-flight charging under improved technology levels.

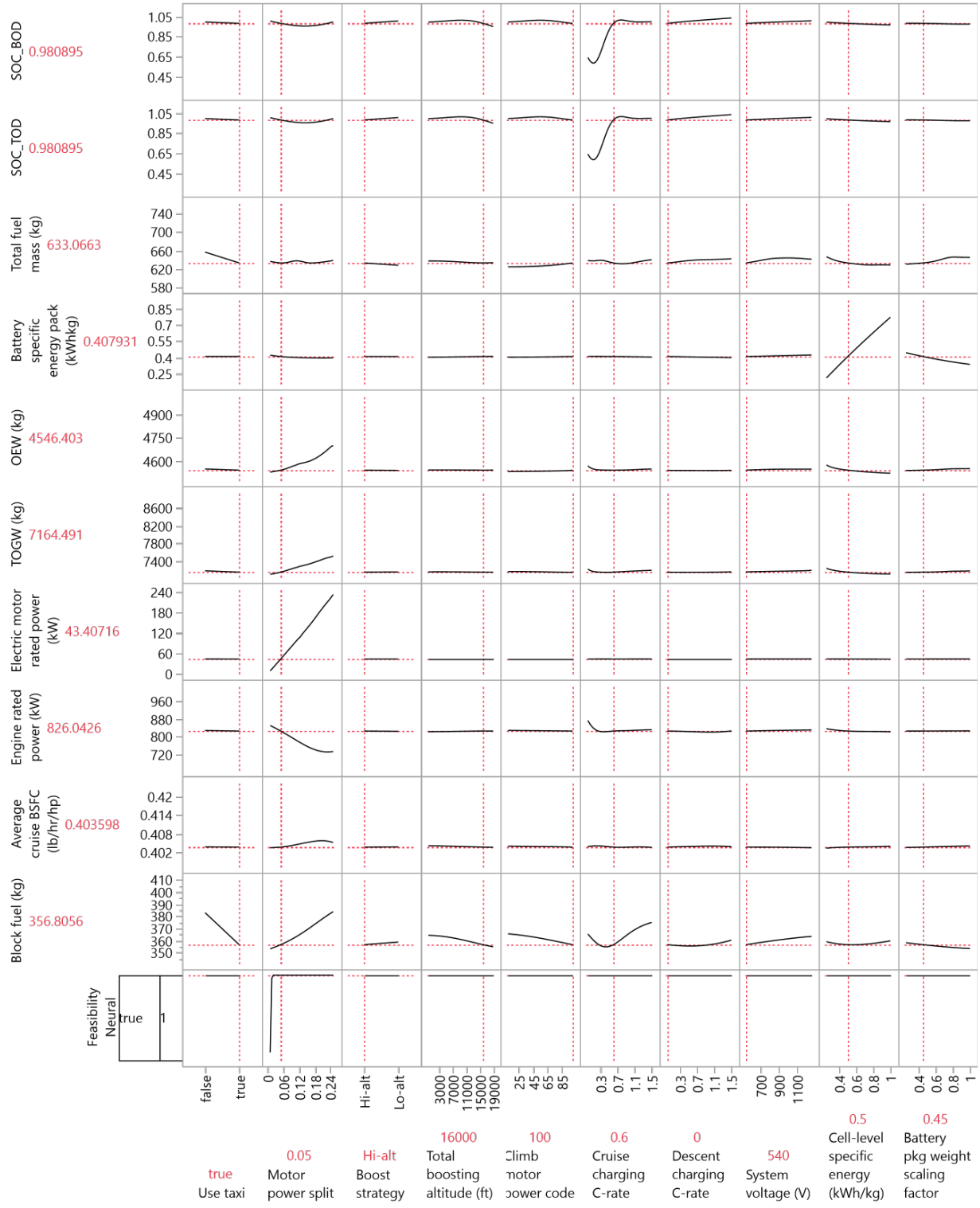

Fig. 28 Part 1 of the full profiler for 19-pax Scenario III with e-taxi and in-flight charging. 2030 technology assumptions.

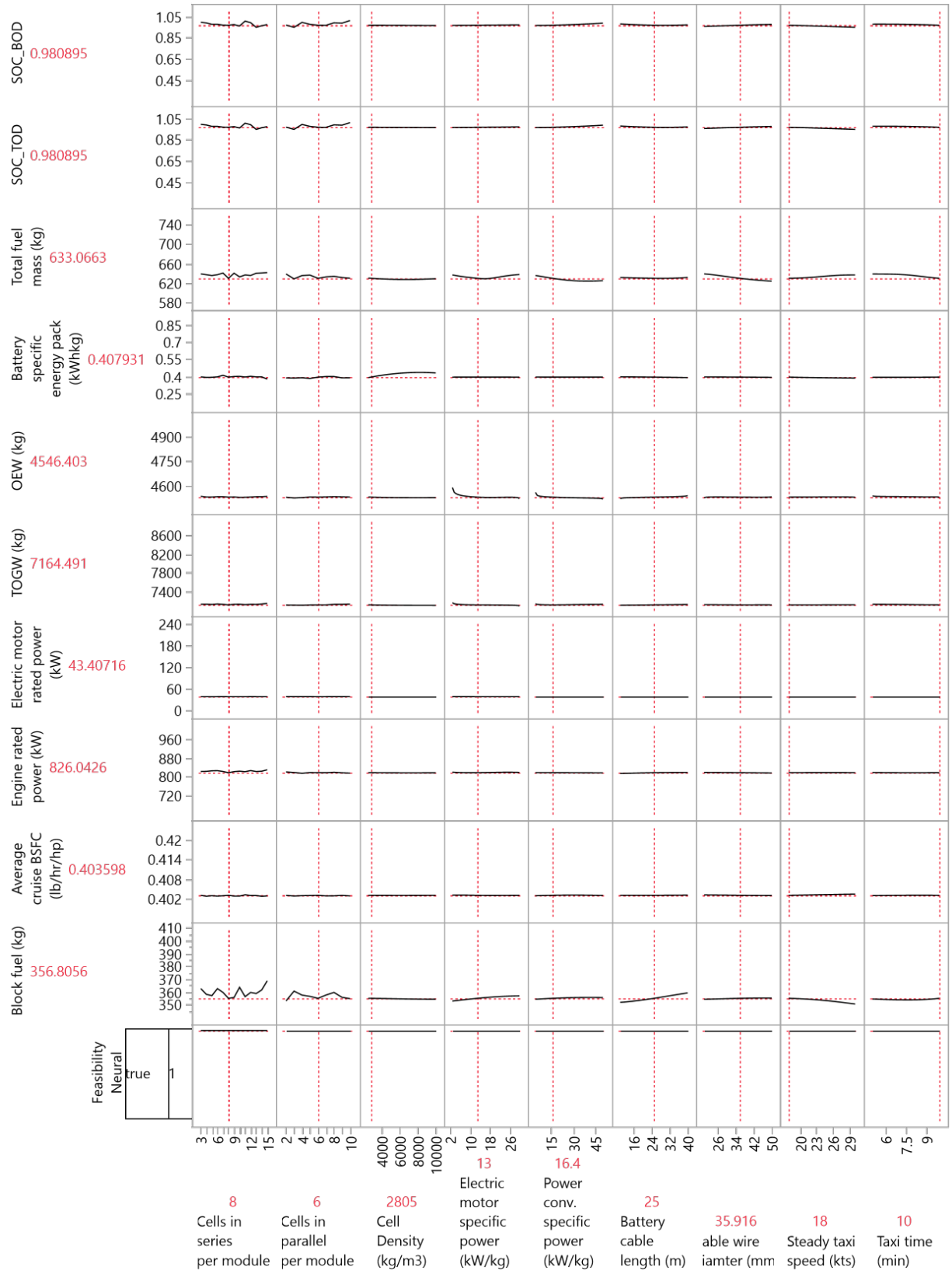

Fig. 29 Part 2 of the full profiler for 19-pax Scenario III with e-taxi and in-flight charging. 2030 technology assumptions.

References

[1] Miranda, D., "2020 NASA Technology Taxonomy," Tech. Rep. HQ-E-DAA-TN76545, NASA, Jan. 2020. URL https://ntrs.nasa.gov/citations/20200000399.

[2] Borer, N. K., Nickol, C. L., Jones, F., Yasky, R., Woodham, K., Fell, J., Litherland, B., Loyselle, P., Provenza, A., Kohlman, L., et al., "Overcoming the adoption barrier to electric flight," *54th AIAA Aerospace Sciences Meeting*, 2016, p. 1022. https://doi.org/10.2514/6.2016-1022.

[3] Bills, A., Sripad, S., Fredericks, W. L., Singh, M., and Viswanathan, V., "Performance Metrics Required of Next-Generation Batteries to Electrify Commercial Aircraft," *ACS Energy Letters*, Vol. 5, No. 2, 2020, pp. 663–668. https://doi.org/10.1021/acsenergylett.9b02574.

[4] Gladin, J. C., Trawick, D., Perullo, C., Tai, J. C., and Mavris, D. N., "Modeling and Design of a Partially Electric Distributed Aircraft Propulsion System with GT-HEAT," *55th AIAA Aerospace Sciences Meeting*, 2017. https://doi.org/10.2514/6.2017-1924.

[5] Markov, A., Cinar, G., Gladin, J. C., Garcia, E., Denney, R. K., Patnaik, S. S., and Mavris, D. N., *Performance Assessment of a Distributed Electric Propulsion System for a Medium Altitude Long Endurance Unmanned Aerial Vehicle*, 2021. https://doi.org/10.2514/6.2021-3289.

[6] Bendarkar, M. V., Sarojini, D., and Mavris, D. N., "Off-Nominal Performance and Reliability of Novel Aircraft Concepts During Early Design," *Journal of Aircraft*, Vol. 59, No. 2, 2022, pp. 400–414. https://doi.org/10.2514/1.C036395.

[7] Bendarkar, M. V., "An Integrated Framework to Evaluate Off-Nominal Requirements and Reliability of Novel Aircraft Architectures in Early Design," Ph.D. thesis, Georgia Institute of Technology, 2021. URL http://hdl.handle.net/1853/64762.

[8] de Vries, R., Hoogreef, M. F. M., and Vos, R., "Range Equation for Hybrid-Electric Aircraft with Constant Power Split," *Journal of Aircraft*, Vol. 57, No. 3, 2020, pp. 552–557. https://doi.org/10.2514/1.C035734.

[9] Wroblewski, G. E., and Ansell, P. J., "Mission Analysis and Emissions for Conventional and Hybrid-Electric Commercial Transport Aircraft," *Journal of Aircraft*, Vol. 56, No. 3, 2019, pp. 1200–1213. https://doi.org/10.2514/1.C035070.

[10] Pornet, C., Gologan, C., Vratny, P. C., Seitz, A., Schmitz, O., Isikveren, A. T., and Hornung, M., "Methodology for Sizing and Performance Assessment of Hybrid Energy Aircraft," *Journal of Aircraft*, Vol. 52, No. 1, 2015, pp. 341–352. https://doi.org/10.2514/1.C032716.

[11] Voskuijl, M., Van Bogaert, J., and Rao, A. G., "Analysis and design of hybrid electric regional turboprop aircraft," *CEAS Aeronautical Journal*, Vol. 9, No. 1, 2018, pp. 15–25. https://doi.org/10.1007/s13272-017-0272-1.

[12] IEA, "ETP Clean Energy Technology Guide," Interactive framework, November 2021. URL https://www.eia.gov/outlooks/aeo/pdf/aeo2020.pdf.

[13] Marien, T., Blaesser, N. J., Frederick, Z. J., Guynn, M. D., Kirk, J., FIsher, K., Schneider, S., Thacker, R. P., and Frederic, P., "Methodology Used for an Electrified Aircraft Propulsion Design Exploration," *AIAA AVIATION 2021 FORUM*, 2021, p. 3191. https://doi.org/10.2514/6.2021-3191.

[14] Marien, T., Blaesser, N., Frederick, Z., Guynn, M., Kirk, J., Fisher, K., Schneider, S. J., Thacker, R., and Frederic, P., "Results for an Electrified Aircraft Propulsion Design Exploration," *AIAA Propulsion and Energy 2021 Forum*, 2021, p. 3280. https://doi.org/10.2514/6.2021-3280.

[15] Jansen, R., Brown, G. V., Felder, J. L., and Duffy, K. P., "Turboelectric aircraft drive key performance parameters and functional requirements," *51st AIAA/SAE/ASEE joint propulsion conference*, 2015, p. 3890. https://doi.org/10.2514/6.2015-3890.

[16] Duffy, K. P., and Jansen, R. H., "Turboelectric and Hybrid Electric Aircraft Drive Key Performance Parameters," *2018 AIAA/IEEE Electric Aircraft Technologies Symposium (EATS)*, IEEE, 2018, pp. 1–19. https://doi.org/10.2514/6.2018-5023.

[17] Dean, T. S., Wroblewski, G. E., and Ansell, P. J., "Mission analysis and component-level sensitivity study of hybrid-electric general-aviation propulsion systems," *Journal of Aircraft*, Vol. 55, No. 6, 2018, pp. 2454–2465. https://doi.org/10.2514/1.C034635.

[18] De Vries, R., Brown, M., and Vos, R., "Preliminary sizing method for hybrid-electric distributed-propulsion aircraft," *Journal of Aircraft*, Vol. 56, No. 6, 2019, pp. 2172–2188. https://doi.org/10.2514/1.C035388.

[19] Finger, D. F., Bil, C., and Braun, C., "Initial sizing methodology for hybrid-electric general aviation aircraft," *Journal of Aircraft*, Vol. 57, No. 2, 2020, pp. 245–255. https://doi.org/doi.org/10.2514/1.C035428.

[20] Chakraborty, I., and Mishra, A. A., "Generalized Energy-Based Flight Vehicle Sizing and Performance Analysis Methodology," *Journal of Aircraft*, Vol. 58, No. 4, 2021, pp. 762–780. https://doi.org/10.2514/1.C036101.

[21] Isikveren, A. T., "Method of quadrant-based algorithmic nomographs for hybrid/electric aircraft predesign," *Journal of Aircraft*, Vol. 55, No. 1, 2018, pp. 396–405. https://doi.org/10.2514/1.C034355.

[22] Ma, Y., Zhang, W., Zhang, Y., Zhang, X., and Zhong, Y., "Sizing method and sensitivity analysis for distributed electric propulsion aircraft," *Journal of Aircraft*, Vol. 57, No. 4, 2020, pp. 730–741. https://doi.org/10.2514/1.C035581.

[23] Cinar, G., Cai, Y., Chakraborty, I., and Mavris, D. N., "Sizing and optimization of novel general aviation vehicles and propulsion system architectures," *2018 Aviation Technology, Integration, and Operations Conference*, 2018, p. 3974. https://doi.org/10.2514/6.2018-3974.

[24] Finger, D. F., de Vries, R., Vos, R., Braun, C., and Bil, C., "Cross-Validation of Hybrid-Electric Aircraft Sizing Methods," *Journal of Aircraft*, 2022, pp. 1–19. https://doi.org/10.2514/1.C035907.

[25] Jansen, R., Kiris, C. C., Chau, T., Machado, L. M., Duensing, J. C., Mirhashemi, A., Chapman, J., French, B. D., Miller, L., Litt, J. S., et al., "Subsonic Single Aft Engine (SUSAN) Transport Aircraft Concept and Trade Space Exploration," *AIAA SCITECH 2022 Forum*, 2022, p. 2179. https://doi.org/10.2514/6.2022-2179.

[26] Spierling, T., and Lents, C., "Parallel hybrid propulsion system for a regional turboprop: conceptual design and benefits analysis," *2019 AIAA/IEEE Electric Aircraft Technologies Symposium (EATS)*, IEEE, 2019, pp. 1–7. https://doi.org/10.2514/6.2019-4466.

[27] Gladin, J. C., Perullo, C., Tai, J. C., and Mavris, D. N., "A Parametric Study of Hybrid Electric Gas Turbine Propulsion as a Function of Aircraft Size Class and Technology Level," *55th AIAA Aerospace Sciences Meeting*, 2017. https://doi.org/10.2514/6.2017-0338.

[28] Graver, B., Zhang, K., and Rutherford, D., "CO_2 emissions from commercial aviation, 2018," International Council on Clean Transportation, 2019. URL https://theicct.org/wp-content/uploads/2021/06/ICCT_CO2-commercl-aviation-2018_20190918.pdf.

[29] Air Transport Action Group, "Waypoint 2050," online, 2020. URL https://aviationbenefits.org/media/167187/w2050_full.pdf.

[30] Cai, Y., Xie, J. X., Cinar, G., and Mavris, D. N., "Advanced 2030 Turboprop Aircraft Modeling for the Electrified Powertrain Flight Demonstration Program," *2022 IEEE/AIAA Transportation Electrification Conference and Electric Aircraft Technologies Symposium (ITEC+EATS)*, IEEE, 2022. https://doi.org/10.1109/ITEC53557.2022.9813858.

[31] Harish, A., Shi, M., Gladin, J., and Mavris, D. N., "Advanced 2030 Single Aisle Aircraft Modeling for the Electrified Powertrain Flight Demonstration Program," *2022 IEEE/AIAA Transportation Electrification Conference and Electric Aircraft Technologies Symposium (ITEC+EATS)*, IEEE, 2022. https://doi.org/10.1109/ITEC53557.2022.9813859.

[32] Cinar, G., Cai, Y., Denney, R. K., and Mavris, D. N., "Modeling and Simulation of a Parallel Hybrid Electric Regional Aircraft for the Electrified Powertrain Flight Demonstration (EPFD) Program," *2022 IEEE/AIAA Transportation Electrification Conference and Electric Aircraft Technologies Symposium (ITEC+EATS)*, IEEE, 2022. https://doi.org/10.1109/ITEC53557.2022.9813832.

[33] Gladin, J., Jr., J. K., Brooks, J., Burrell, A., Hall, C., Milios, K., and Mavris, D. N., "Modeling and Simulation of a Parallel Hybrid-Electric Propulsion System - Electrified Powertrain Flight Demonstration (EPFD) Program," *2022 IEEE/AIAA Transportation Electrification Conference and Electric Aircraft Technologies Symposium (ITEC+EATS)*, IEEE, 2022. https://doi.org/10.1109/ITEC53557.2022.9813981.

[34] Kratz, J., Connolly, J., Amthor, A., Buescher, H., Bianco, S., and Culley, D., "Turbine Electrified Energy Management for Single Aisle Aircraft," *2022 IEEE Transportation Electrification Conference Expo (ITEC)*, 2022, pp. 658–663. https://doi.org/10.1109/ITEC53557.2022.9813818.

[35] Pastra, C. L., Hall, C., Cinar, G., Gladin, J., and Mavris, D. N., "Specific Power and Efficiency Projections of Electric Machines and Circuit Protection Exploration for Aircraft Applications," *2022 IEEE/AIAA Transportation Electrification Conference and Electric Aircraft Technologies Symposium (ITEC+EATS)*, IEEE, 2022. https://doi.org/10.1109/ITEC53557.2022.9813927.

[36] Hall, C., Pastra, C. L., Burrell, A., Gladin, J., and Mavris, D. N., "Projecting Power Converter Specific Power Through 2050 for Aerospace Applications," *2022 IEEE/AIAA Transportation Electrification Conference and Electric Aircraft Technologies Symposium (ITEC+EATS)*, IEEE, 2022. https://doi.org/10.1109/ITEC53557.2022.9813991.

[37] Tiede, B., O'Meara, C., and Jansen, R., "Battery Key Performance Projections Based on Historical Trends and Chemistries," *2022 IEEE/AIAA Transportation Electrification Conference and Electric Aircraft Technologies Symposium (ITEC+EATS)*, IEEE, 2022. https://doi.org/10.1109/ITEC53557.2022.9814008.

[38] Dever, T., and Jansen, R., "Cable Key Performance Parameters for Megawatt Electrified Aircraft Propulsion Conceptual Aircraft Model," *2022 IEEE/AIAA Transportation Electrification Conference and Electric Aircraft Technologies Symposium (ITEC+EATS)*, IEEE, 2022. https://doi.org/10.1109/ITEC53557.2022.9814005.

[39] Cinar, G., "A methodology for dynamic sizing of electric power generation and distribution architectures," Ph.D. thesis, Georgia Institute of Technology, 2018. URL http://hdl.handle.net/1853/60754.

[40] Cinar, G., Garcia, E., and Mavris, D. N., "A framework for electrified propulsion architecture and operation analysis," *Aircraft Engineering and Aerospace Technology*, Vol. 92, No. 5, 2019, pp. 675–684. https://doi.org/10.1108/AEAT-06-2019-0118.

[41] McCullers, L., *Flight Optimization System, Release 8.11, User's Guide*, NASA Langley Research Center, Hampton, VA 23681-0001, Oct. 2009.

[42] Wells, D. P., Horvath, B. L., and McCullers, L. A., "The Flight Optimization System Weights Estimation Method," Tech. Rep. NASA/TM-2017-219627/VOL1, NASA, Jun. 2017.

[43] Cai, Y., Rajaram, D., and Mavris, D. N., "Multi-mission Multi-objective Optimization in Commercial Aircraft Conceptual Design," *AIAA Aviation 2019 Forum*, American Institute of Aeronautics and Astronautics, 2019. https://doi.org/10.2514/6.2019-3577.

[44] Cai, Y., Rajaram, D., and Mavris, D. N., "Simultaneous Aircraft Sizing and Multi-Objective Optimization Considering Off-Design Mission Performance during Early Design," *Aerospace Science and Technology*, 2022, p. 107662. https://doi.org/https://doi.org/10.1016/j.ast.2022.107662, URL https://www.sciencedirect.com/science/article/pii/S1270963822003364.

[45] Lytle, J. K., "The Numerical Propulsion System Simulation: An Overview," Tech. Rep. NASA/TM-2000-209915, National Aeronautics and Space Administration, Glenn Research Center, Cleveland, OH, June 2000.

[46] Snyder, C. A., and Tong, M. T., "Modeling Turboshaft Engines for the Revolutionary Vertical Lift Technology Project," Tech. Rep. GRC-E-DAA-TN66991, NASA, May 2019. URL https://ntrs.nasa.gov/citations/20190025407.

[47] Bettner, J., "Component arrangement studies for an 8000 shp turboshaft high technology core," *26th Joint Propulsion Conference*, 1990, p. 2398. https://doi.org/10.2514/6.1990-2398.

[48] Vogt, R. L., and Sehra, A., "Next Generation 2 MW Turboshaft and Turboprop Engines," *Turbo Expo: Power for Land, Sea, and Air*, Vol. 78880, American Society of Mechanical Engineers, 1993, p. V001T01A005. https://doi.org/10.1115/93-GT-046.

[49] Gauntner, J. W., "Algorithm for Calculating Turbine Cooling Flow and the Resulting Decrease in Turbine Efficiency," Tech. Rep. NASA/TM-81453, National Aeronautics and Space Administration, 1980.

[50] Schutte, J. S., "Simultaneous multi-design point approach to gas turbine on-design cycle analysis for aircraft engines," Ph.D. thesis, Georgia Institute of Technology, 2009.

[51] "ASN Aviation Safety Database," online, May 2021. URL https://aviation-safety.net/database/.

[52] "TYPE-CERTIFICATE DATA SHEET for PT6A-67 Series Engines," online, Oct. 2019. URL https://www.easa.europa.eu/sites/default/files/dfu/PT6A_67SeriesIssue05_20191011.pdf.

[53] "TYPE-CERTIFICATE DATA SHEET for PW100 series engines," online, Mar. 2018. URL https://www.easa.europa.eu/sites/default/files/dfu/EASAIM.E.041TCDSIssue4.pdf.

[54] "ATR Family," online, Sep. 2011. URL http://www.aeropolis.it/workshop2018/Seminario2018-9giugno/DocumentazionePresentazioni/ATRFAMILY-LivretATR2011.pdf.

[55] *Model 1900D Airliner Pilot's Operating Manual*, Hawker Beechcraft Corporation, P.O. Box 85, Wichita, Kansas, 67201-0085 USA, Sep. 2008.

[56] Mavris, D. N., Tai, J., and Gladin, J., "FY2019 Advanced Air Transportation TechnologiesSystems Analysis Report: Technology Portfolio," techreport, Georgia Institute of Technology, Jul. 2020.

[57] Catalano, P., de Rosa, D., Mele, B., Tognaccini, R., and Moens, F., "Performance Improvements of a Regional Aircraft by Riblets and Natural Laminar Flow," *Journal of Aircraft*, Vol. 57, No. 1, 2020, pp. 29–40. https://doi.org/10.2514/1.c035445.

[58] Mavris, D., and Schutte, J. S., *Application of deterministic and probabilistic system design methods and enhancements of conceptual design tools for era project*, National Aeronautics and Space Administration, Langley Research Center, 2016.

[59] ATR, "ATR-42-600," Brochure, 2015. URL https://skybrary.aero/bookshelf/books/3695.pdf.

[60] Larminie, J., and Lowry, J., *Electric vehicle technology explained*, John Wiley & Sons, 2012.

[61] Tremblay, O., and Dessaint, L.-A., "Experimental validation of a battery dynamic model for EV applications," *World electric vehicle journal*, Vol. 3, No. 2, 2009, pp. 289–298. https://doi.org/10.3390/wevj3020289.

[62] Campbell, A. M., "Architecting aircraft power distribution systems via redundancy allocation," Ph.D. thesis, Georgia Institute of Technology, 2014. URL http://hdl.handle.net/1853/53087.

[63] *NFPA 70, National Electrical Code (NEC)*, National Fire Protection Association, 2017.

[64] Hamilton Standard, "Generalized Method of Propeller Performance Estimation 1961-1963," , 1963. URL https://open.bu.edu/handle/2144/10454.

[65] Gudmundsson, S., "The Anatomy of the Propeller," *General Aviation Aircraft Design*, Elsevier, 2014, pp. 581–659. https://doi.org/10.1016/b978-0-12-397308-5.00014-3.

[66] Yann, N., "eTaxi: Taxiing aircraft with engines stopped," *Flight Airworthiness Support Technology, Airbus Technical Magazine*, Vol. 51, 2013.

[67] "Advisory Circular 150/5300-13A, Airport Design," *Federal Aviation Administration*, 2014. Online: https://www.faa.gov/documentLibrary/media/Advisory_Circular/150-5300-13A-chg1-interactive-201907.pdf, accessed Feb. 18, 2021.

[68] Shi, M., Cinar, G., and Mavris, D., "Fleet Analysis of a Hybrid Turboelectric Commercial Regional Jet under NASA ULI Program," *AIAA Propulsion and Energy 2021 Forum*, 2021. https://doi.org/10.2514/6.2021-3327.